Radiolabeled inhibitors as probes for imaging mutant IDH1 expression in gliomas: Synthesis and preliminary evaluation of labeled butyl-phenyl sulfonamide analogs

Satish K. Chitneni, Zachary J. Reitman, David M. Gooden, Hai Yan, Michael R. Zalutsky

PII: S0223-5234(16)30359-2
DOI: doi:10.1016/j.ejmech.2016.04.066
Reference: EJMECH 8581

Published in: *European Journal of Medicinal Chemistry*

Received date: 22 February 2016
Revised date: 25 April 2016
Accepted date: 26 April 2016

Cite this article as: Chitneni SK, Reitman ZJ, Gooden DM, Yan H, Zalutsky MR, Radiolabeled inhibitors as probes for imaging mutant IDH1 expression in gliomas: Synthesis and preliminary evaluation of labeled butyl-phenyl sulfonamide analogs, *European Journal of Medicinal Chemistry*, doi:10.1016/j.ejmech.2016.04.066

Graphical Abstract

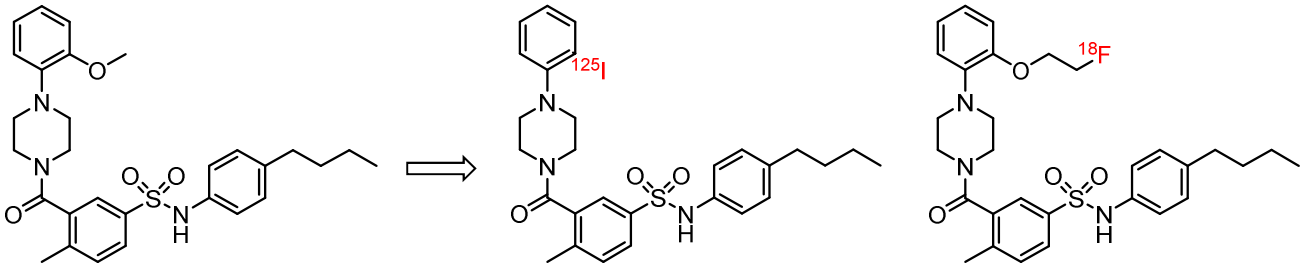

A
Mutant IDH1 inhibitor
IC_{50}: 2.2 μM

[^{125}I]**1**
IC_{50}: 1.7 μM

[^{18}F]**4**
IC_{50}: 2.3 μM

Radiolabeled inhibitors as probes for imaging mutant IDH1 expression in gliomas: synthesis and preliminary evaluation of labeled butyl-phenyl sulfonamide analogs

Satish K. Chitneni[1], Zachary J. Reitman[2], David M. Gooden[3], Hai Yan[2], Michael R. Zalutsky[1]

[1]Department of Radiology, [2]Department of Pathology, Duke University Medical Center, Durham, NC 27710, USA; [3]Small Molecule Synthesis Facility, Duke University, Durham, NC 27708, USA.

Corresponding author:

Satish K. Chitneni

Box 3808

Department of Radiology

Duke University Medical Center

Durham

NC 27710

USA

E-mail: satish.chitneni@duke.edu

ABSTRACT

Introduction: Malignant gliomas frequently harbor mutations in the isocitrate dehydrogenase 1 (IDH1) gene. Studies suggest that IDH mutation contributes to tumor pathogenesis through mechanisms that are mediated by the neomorphic metabolite of the mutant IDH1 enzyme, 2-hydroxyglutarate (2-HG). The aim of this work was to synthesize and evaluate radiolabeled compounds that bind to the mutant IDH1 enzyme with the goal of enabling noninvasive imaging of mutant IDH1 expression in gliomas by positron emission tomography (PET).

Methods: A small library of nonradioactive analogs were designed and synthesized based on the chemical structure of reported butyl-phenyl sulfonamide inhibitors of mutant IDH1. Enzyme inhibition assays were conducted using purified mutant IDH1 enzyme, IDH1-R132H, to determine the IC_{50} and the maximal inhibitory efficiency of the synthesized compounds. Selected compounds, **1** and **4**, were labeled with radioiodine (^{125}I) and/or ^{18}F using bromo- and phenol precursors, respectively. In vivo behavior of the labeled inhibitors was studied by conducting tissue distribution studies with [^{125}I]**1** in normal mice. Cell uptake studies were conducted using an isogenic astrocytoma cell line that carried a native IDH1-R132H mutation to evaluate the potential uptake of the labeled inhibitors in IDH1-mutated tumor cells.

Results: Enzyme inhibition assays showed good inhibitory potency for compounds that have iodine or a fluoroethoxy substituent at the *ortho* position of the phenyl ring in compounds **1** and **4** with IC_{50} values of 1.7 µM and 2.3 µM, respectively. Compounds **1** and **4** inhibited mutant IDH1 activity and decreased the production of 2-HG in an IDH1-mutated astrocytoma cell line. Radiolabeling of **1** and **4** was achieved with an average radiochemical yield of 56.6 ± 20.1% for [^{125}I]**1** (n=4) and 67.5 ± 6.6% for [^{18}F]**4** (n=3). [^{125}I]**1** exhibited favorable biodistribution characteristics in normal mice, with rapid clearance from the blood and elimination via the hepatobiliary system by 4 h after injection. The uptake of [^{125}I]**1** in tumor cells positive for IDH1-R132H was significantly higher compared to isogenic WT-IDH1 controls, with a maximal uptake

ratio of 1.67 at 3 h post injection. Co-incubation of the labeled inhibitors with the corresponding nonradioactive analogs, and decreasing the normal concentrations of FBS (10%) in the incubation media substantially increased the uptake of the labeled inhibitors in both the IDH1-mutant and WT-IDH1 tumor cell lines, suggesting significant non-specific binding of the synthesized labeled butyl-phenyl sulfonamide inhibitors.

Conclusions: These data demonstrates the feasibility of developing radiolabeled probes for the mutant IDH1 enzyme based on enzyme inhibitors. Further optimization of the labeled inhibitors by modifying the chemical structure to decrease the lipophilicity and to increase potency may yield compounds with improved characteristics as probes for imaging mutant IDH1 expression in tumors.

Keywords: IDH mutation, glioma, mutant IDH1 inhibitor, PET imaging, fluorine-18, radioiodine

INTRODUCTION

Isocitrate dehydrogenase 1 encodes for the IDH1 enzyme, which plays important roles in cellular metabolism, energy production and maintenance of normal redox status in cells. IDH1 is localized in the cell cytoplasm and peroxisomes where it catalyzes the conversion of isocitrate to α-ketoglutarate (α-KG) and simultaneously reduces NADP to NADPH [1]. α-Ketoglutarate serves as a key intermediate in the tricarboxylic acid cycle (TCA) in cells, and as substrate for several important dioxygenase enzymes. NADPH is a key cofactor in the cholesterol and lipid synthesis pathways and also contributes to cell defense against oxidative damage induced by reactive oxygen species (ROS) [2]. Recent genome-wide mutation analysis studies revealed that gliomas frequently harbor mutations in IDH1 and, to a lesser extent, the homologous IDH2 genes [3, 4]. IDH1 mutations are present in over 75% of WHO grade 2 and grade 3 gliomas and in secondary gliomas that develop from lower-grade tumors [2, 4, 5]. IDH mutations are generally associated with better prognosis when compared to glioma patients with wild-type IDH (WT-IDH) tumors of the same histological type [4, 6]. The median overall survival of patients with IDH-mutated glioblastoma and anaplastic astrocytoma is approximately 2-3 times longer than for patients whose tumors have WT-IDH1 [4], strongly suggesting the prognostic significance of IDH1 and IDH2 mutations in glioma [7].

Studies suggest that IDH mutations also play significant roles in tumorigenesis. IDH mutation is an early genetic event in the formation of gliomas, and contributes to tumor pathogenesis through multiple mechanisms that are mediated by the neomorphic activity of the mutated IDH1 enzyme [5, 8, 9]. IDH mutation results in a loss of normal catalytic activity - conversion of isocitrate to α-KG - for the IDH enzyme but also imparts a new gain-of-function that enables the mutant IDH to convert α-KG to 2-hydroxyglutarate (2-HG) in a stereospecific manner (D-2-HG) [10]. Consequently, tumors that are positive for IDH1 mutation have ~100-fold higher levels of D-2-HG compared to tumors with normal IDH1 (WT-IDH1). Excessive D-2-HG in IDH1-mutated cells competitively inhibits several key cellular dioxygenases that are normally dependent on α-

KG as a co-factor for their enzyme activity [11]. This competitive inhibition is presumed to be due to the structural similarity of D-2-HG with the α-KG, and results in the impairment of the activity of multiple cellular dioxygenases leading to stabilization and activation of the transcription factor hypoxia-inducible factor-1α (HIF-1α), epigenetic dysregulation leading to histone methylation and DNA hypermethylation, and impairment of normal collagen maturation [12-14]. IDH1 mutations also directly impact the cellular metabolism of small biochemicals such as amino acids, glutathione derivatives and tricarboxylic acid (TCA) cycle intermediates, suggesting the occurrence of widespread metabolic changes in IDH1-mutated tumor cells [15, 16].

In view of these diverse roles and the impact of IDH1 mutations on cellular metabolism and epigenetics, there is a strong rationale for development of noninvasive imaging methods (e.g. PET) to evaluate mutant IDH1 expression in gliomas. Such a method could enable determination of the IDH1 mutation status in glioma patients noninvasively, predict prognosis and assist in the design and implementation of novel therapeutics for patients with malignant brain tumors as well as other cancers that carry these mutations [2, 5]. In this work, we have synthesized and evaluated radiolabeled compounds that have inhibitory activity against the most commonly occurring IDH1 mutation subtype, IDH1-R132H [17]. Selected compounds were labeled with radioiodine and/or fluorine-18, and in vitro studies and preliminary in vivo studies were conducted using the labeled inhibitors in order to assess their suitability as probes for mutant IDH1.

RESULTS AND DISCUSSION

Chemistry

Butyl-phenyl sulfonamide inhibitors of mutant IDH were among the first compounds shown to inhibit mutant IDH1 activity in vitro. From this chemical class, *N*-(4-butylphenyl)-3-(4-(2-methoxyphenyl)piperazine-1-carbonyl)-4-methylbenzenesulfonamide **A** (**Fig. 1**) was chosen as

the reference compound, which has an IC_{50} value of <1 µM against the mutant IDH1-R132H enzyme [17]. A series of nonradioactive iodo- and/or fluorinated analogs of **A** were synthesized for structure-activity relationship studies and to identify potent inhibitors for radiolabeling (**Fig. 2**). The basic synthesis route involved the reaction of commercially available 5-(*N*-(4-butylphenyl)sulfamoyl)-2-methylbenzoic acid with appropriate phenyl piperazine derivative in the presence of the coupling reagents EDC and HOBt in DMF (**Scheme 1**) [17]. For the iodophenyl analogs **1** and **2**, the piperazine derivatives 1-(2-iodophenyl)piperazine and 1-(4-iodophenyl)piperazine were synthesized following a literature report [17], and were subsequently coupled to the benzoic acid derivative in 62% yield for **1** and 71% yield for **2**. The fluoroethyl analogs **4** and **5** were synthesized by introduction of a fluoroethoxy function at the *ortho*- or *para*- position of the phenyl ring in the phenyl piperazine moiety. For these reactions, fluoroethoxyphenyl piperazine derivatives were synthesized by using the corresponding phenol piperazine via a 3-step synthesis route [18]. First, the secondary amine function in the piperazine ring was protected with a Boc-group in quantitative yields. Fluoroethylation of the boc-protected 2- or 4-hydroxypheyl piperazine was achieved by using fluoroethyl bromide (FEtBr) in about 75% yield. Removal of the boc protective groups with a mixture of TFA and CH_2Cl_2 (50/50, v/v) yielded the fluoroethoxyphenyl piperazine derivatives in quantitative yields. The synthesized 2- and 4-fluoroethoxyphenyl piperazine analogs were then reacted with the methylbenzoic acid derivative to obtain the fluoroethoxy analogs **4** and **5** in 40-47% yield (**Scheme 1**). For compound **3**, the iodine atom was introduced in place of the methyl group in the methylbenzoic acid derivative in a two-step synthesis (**9**) and was then coupled to 1-(-2-methoxyphenyl)piperazine in 59% yield (**Scheme 2**).

Scheme 3 shows the synthesis route for the fluoroalkyl derivatives **6** and **7**. Introduction of the fluorine atom into the side chain in these compounds was achieved by means of a fluorpropyl (**6**) or a fluorobutyl (**7**) function. For these syntheses, the fluoroalkyl aniline derivatives **12a** and

12b were synthesized first, and were subsequently reacted with 5-(chlorosulfonyl)-2-methylbenzoic acid to obtain **13a** or **13b**. The synthesis of 4-(3-fluoropropyl)aniline **12a** was achieved using commercially available 3-(4-nitrophenyl)propionic acid (structure not shown) where the carboxylic acid function was first reduced to an alcohol using borane in THF to get **10a**. Treatment of the alcohol derivatives **10a** and **10b** with XTalFluor-M in the presence of DBU as the promotor yielded the fluoroalkyl-nitrobenzene analogs **11a** and **11b** in 41% and 53% yield, respectively (**Scheme 3**). Reduction of the nitro group to an amino function by Pd/C-catalized hydrogenation followed by sulfamoylation of the anilines with 5-(chlorosulfonyl)-2-methylbenzoic afforded the fluoroalkylphenyl sulfonamide intermediates **13a** and **13b** in 69-74% yield. Compounds **13a** and **13b** were then coupled to 1-(2-methoxyphenyl)piperazine to obtain the final compounds **6** and **7** in 85% and 78% yield, respectively. The synthesis of the radiolabeling precursors **14** and **15** was achieved as described for **1** using 1-(2-bromophenyl)piperazine and 2-(piperazin-1-yl)phenol as starting materials and with a chemical yield of 77% and 54%, respectively. The synthesized compounds were evaluated by mass spectrometry for identity confirmation and characterized by NMR spectroscopy. The purity of the synthesized nonradioactive analogs and the radiolabeling precursors was verified by analytical HPLC, and was found to be between 94% and 98%.

Inhibitory Activity of the Nonradioactive Analogs against the Mutant IDH1

The inhibitory activity of the nonradioactive iodo- and fluoro analogs was evaluated by incubating serially-diluted (2-fold) solutions of the compounds with purified IDH1-R132H enzyme in multiwell plates. **Figure 2** shows the half-maximal inhibitory concentration (IC_{50}) values and the maximal enzyme inhibition achieved for the synthesized compounds in the inhibition assays. **Figure 3** shows the inhibitory curves derived from these experiments for the reference methoxy analog **A** and for some of the unlabeled inhibitors synthesized in this work, at 0.19 – 392 μM concentrations. The results showed that the substitution of the *ortho*-methoxy group in the

reference compound **A** with an iodine atom or a fluoroethoxy function did not affect inhibitory potency for compounds **1** and **4** against the mutant IDH1. The IC_{50} of **1** and **4** against the mutant IDH1 in these experiments was 1.7 and 2.3 µM, respectively, as compared to 2.2 µM for the reference Compound **A**. The inhibitory efficiency of **1** and **4** in terms of maximal enzyme inhibition also was similar to that for the reference methoxy analog, all showing near-complete inhibition (100%) of mutant IDH1 activity in the tested concentration range (0.19 – 392 µM). On the other hand, substitution of an iodo- or fluoroethoxy function at the *para* position of the phenyl ring resulted in a substantial decrease in potency for compounds **2** and **5** against mutant IDH1. While the *para*-fluoroethoxy derivative **5** displayed partial inhibitory activity with an IC_{50} of 1.2 µM but a maximum enzyme inhibition of only ~30%, the *para*-iodo analog **2** did not show any significant activity against mutant IDH1, suggesting that the structural modification at the *para*-position was not well-tolerated for the binding affinity. Introduction of a fluorine atom in place of hydrogen or the terminal methyl group in the butyl side chain also resulted in good retention of inhibitory activity for compounds **6** and **7**, with IC_{50} values of 2.7 µM and 2.4 µM, and an inhibitory efficiency of 99% and 81%, respectively.

We next evaluated the ability of the nonradioactive compounds to bind to and inhibit mutant IDH1 activity in tumor cells that are positive for the IDH1-R132H mutation. For these experiments, an astrocytoma cell line with a native IDH1-R132H mutation was used [19] with an isogenic astrocytoma cell line with WT-IDH1 serving as a control. Cells were treated with the inhibitors **1** or **4** (50 µM), and the 2-HG concentrations in cell supernatants were analyzed by LC/MS at 4 and 8 h after incubation [14, 19]. Comparison of 2-HG levels in vehicle-treated cell lines showed that the concentration of 2-HG in IDH1-mutated astrocytoma cells was about 30-fold higher than that in isogenic wild-type IDH1 control cells (WT-IDH1), confirming the expression of mutant IDH1 protein and its neomorphic activity in the IDH1-mutated astrocytoma cell line (**Fig. 4**). Addition of the nonradioactive inhibitor **1** or **4** to the culture media decreased 2-HG concentration in mutant IDH1 cell supernatants by 43% for compound **1** and by 50% for

compound **4** at 8 h post-incubation. It is likely that the residual amounts of 2-HG that were present inside the cells prior to their incubation with the inhibitors are exported into the supernatant with time and partially contributed to the concentrations observed at 8 h after incubation with the test compounds. These results are consistent with recent studies that reported a 2-HG inhibitory half-life (50% inhibition) of about 5 h for a structurally unrelated mutant IDH inhibitor [20], and also suggest that incubation times of up to 48 h may be required to achieve complete inhibition of 2-HG production by mutant IDH1 inhibitors in cell based assays [20, 21]. Nevertheless, these results confirm the ability of the unlabeled inhibitors **1** and **4** to inhibit the mutant IDH1 enzyme in tumor cells that are positive for an IDH1 mutation.

Radiochemistry

Radioiodination of **1** ([^{125}I]**1**) was achieved through a Cu(I)-catalyzed Br-to-*I exchange reaction in acidic and reducing conditions using gentisic acid as depicted in **Scheme 4** [22]. After labeling, the crude reaction mixture was purified by RP-HPLC, and the HPLC peak corresponding to the [^{125}I]**1** was further purified by a C_{18} Sep-Pak cartridge in order to remove acetonitrile and TFA from the product before being used for biological experiments. The average radiochemical yield for [^{125}I]**1** was 56.6 ± 20.1% (n=4). ^{18}F labeling of the fluoroethoxy analog **4** was achieved by heating the phenol precursor **14** with the secondary labeling agent [^{18}F]fluoroethyl bromide ([^{18}F]FEtBr) in the presence of cesium carbonate in DMF (**Scheme 5**) [23]. The decay corrected radiochemical yield for [^{18}F]FEtBr synthesis was 48.7 ± 10.8 (n=4), and [^{18}F]**4** was obtained with an average ^{18}F-fluoroethylation efficiency of 67.5 ± 6.6% (n=3). In one synthesis, 1.25 GBq of [^{18}F]**4** was obtained (0.65 GBq at the end of synthesis) starting from 4 GBq of [^{18}F]fluoride, representing an overall radiochemical yield of about 31% relative to initial [^{18}F]fluoride activity. The total synthesis time including HPLC purification was 109 ± 5 min (n=3) for [^{18}F]**4**. The radiochemical purity was >98% for both labeled compounds. Identity confirmation

was achieved by co-elution with the corresponding nonradioactive analogs by analytical HPLC (**Fig. 5**).

Tissue Distribution Studies

Tissue distribution studies were conducted using [^{125}I]**1** in order to evaluate the normal tissue distribution characteristics of the labeled compound and to assess its suitability for development as an imaging agent for mutant IDH1. **Table 1** shows the % ID and **Figure 6** shows the % ID/g values for [^{125}I]**1** in BALB/C mice from 5 min – 4 h post injection. The biodistribution data is consistent with general expectations for a lipophilic small molecule radiotracer, with rapid clearance from the blood and elimination via the hepatobiliary system. At 5 min p.i., about 12% ID was present in the blood, with the activity cleared rapidly with time to about 0.13% ID at 4 h. Except for liver, the activity concentration in the vital organs was < 0.2% ID/g at 4 h, demonstrating good clearance of radioactivity from normal tissues by 4 h. The excretion of the labeled compound thorough kidneys and into urine was minimal with only 3.50 ± 1.08 %ID present in kidneys at 5 min, and a maximum of 2.84% ID excreted into the urine at 1 h. About 30% ID was present in liver at 5 min, with the activity declining with time, most likely reflecting clearance into the intestines. At 2 h, approximately 60% ID was detected in the hepatobiliary system, suggesting this as the major metabolic route for elimination of the labeled inhibitor. The activity concentration (%ID/g) in the thyroid gland at 5 min was 1.69 ± 0.93 but decreased to 0.42 ± 0.16 by 4 h after injection, indicative of the stability of [^{125}I]**1** towards dehalogenation in vivo. The uptake of [^{125}I]**1** in the brain was 0.39 ± 0.13 %ID at 5 min, and remained very low at later time points (≤0.07 %ID/g at 1 – 4 h).

Cell Uptake Studies

The uptake of the labeled inhibitors in mutant IDH expressing cells was evaluated using the same astrocytoma cell line used for the 2-HG inhibition assays by incubating the cells with HPLC-purified [^{125}I]**1** for 15 min – 4 h. At 15 min after incubation, about 0.5% of the added

activity was present in the mutant IDH1 cell line, and increased to 0.80 ± 0.04% at 3 h (P< 0.05). Comparison of the uptake of [^{125}I]**1** in the mutant-IDH1 and WT-IDH1 cell lines revealed an average uptake ratio of 1.66 at 2 h (P< 0.05) and 1.67 at 3 h (P< 0.05) after incubation (**Fig. 7A**). Based on these data, a 3-h incubation was chosen for further studies evaluating the effect of increasing concentrations of unlabeled **1** (0.1 – 100 μM) on cell uptake of [^{125}I]**1** and the binding specificity in mutant IDH1 tumor cells. In these experiments, co-incubation with cold compound resulted in a substantial increase in [^{125}I]**1** uptake in a concentration-dependent manner in both the mutant-IDH1 and WT-IDH1 cell lines (P< 0.05 except for 0.1 μM; **Fig. 7B**). The maximal increase in [^{125}I]**1** uptake was observed at 10 μM **1** where the uptake was 53-fold higher than that for no-carrier-added [^{125}I]**1**, and the uptake decreased at higher concentrations (50 μM and 100 μM). Similarly, decreasing the concentration of the FBS from 10% in the normal incubation media to 0.1% also resulted in increased uptake of [^{125}I]**1** in both the cell lines (**Fig. 7C**). Preliminary evaluation of [^{18}F]**4** also revealed similar results when 10 μM **4** was used for co-incubation experiments. Taken together, these data suggest that the labeled inhibitors undergo significant non-specific binding with increasing concentrations of unlabeled inhibitors and/or with decreasing concentrations of FBS in the incubation media. In part, this non-specific binding can be attributed to the lipophilicity of the labeled inhibitors which have a calculated LogP (cLogP) of 5.94 and 5.15 for the iodo- and fluoroethyl derivatives **1** and **4**, respectively, as compared to 4.93 for the reference methoxy analog **A**. The cLogP of the fluoroalkyl analogs **6** and **7** is somewhat lower, 3.78 and 4.22, respectively, suggesting that radiolabeled analogs of these two compounds may show less non-specific binding compared to that observed for [^{125}I]**1**. In addition to the affinity or the interaction of the labeled molecule with the mutant IDH1 protein, lipophilicity also plays a critical role in the uptake and specific retention of the labeled inhibitors in mutant IDH1 tumor cells. Several PET radiotracers have proven useful for imaging intracellular targets in human gliomas despite their hydrophilic (e.g. [^{18}F]FMISO for hypoxia imaging; cLogP: -0.52) or very lipophilic (e.g. [^{11}C](*R*)-PK11195 for mitochondrial translocator

protein (TSPO) imaging; CLogP: 4.58) [24, 25] characteristics, suggesting practical evaluation of all candidate radiotracers in relevant biological models (in vitro and in vivo) before a lead compound is identified for new imaging targets such as mutant IDH1. While high lipophilicity may increase the risk of non-specific binding of small molecule compounds to proteins, studies suggest that efficient cell membrane permeability requires a LogP of > 0.8 for compounds that are undergoing passive diffusion to enter cells [26]. Using the information obtained from the present study, work is in progress to synthesize and evaluate labeled compounds from additional chemical classes that have been shown to have higher potency than the butyl-phenyl sulfonamide inhibitors and also inhibited the neomorphic activity of mutant IDH1 in tumor models in vivo [21, 27].

Conclusions

A series of nonradioactive mutant IDH1 inhibitors were synthesized based on a butyl-phenyl sulfonamide chemical scaffold. Enzyme inhibition assays using purified IDH1-R132H led to the identification of **1** and **4** as lead compounds for radiolabeling, with IC_{50} of about 2 μM. Radiolabeling of compounds **1** and **4** was achieved using ^{125}I and [^{18}F]fluorethyl bromide, respectively, in good radiochemical yields and purity. Biodistribution studies with [^{125}I]**1** showed favorable normal tissue distribution characteristics; however, cell uptake studies using mutant IDH1 and WT-IDH1 tumor cell lines revealed high nonspecific binding for the labeled inhibitors. Further optimization of these compounds by decreasing the lipophilicity and increasing the inhibitory potency may yield compounds with more favorable uptake characteristics for labeling mutant IDH1 expressing tumor cells with radionuclides suitable for PET imaging.

EXPERIMENTAL SECTION

Reagents and General Methods

The solvents and regents used in this work were purchased from VWR International, LLC, or from Sigma-Aldrich, and were used as supplied. The reference compound *N*-(4-butylphenyl)-3-(4-(2-methoxyphenyl)piperazine-1-carbonyl)-4-methylbenzenesulfonamide (**A**) was purchased from Enamine LLC, New Jersey. Melting points were determined using a Fisher-Johns Melting Point Apparatus. Radioiodine was obtained from PerkinElmer as [^{125}I]NaI solution in 0.1 N NaOH. [^{18}F]Fluoride was supplied by PETNET Solutions (Raleigh-Durham, NC), and was delivered on a Sep-Pak Light Accell plus QMA anion exchange cartridge (Waters). Purification and quality control analysis of the radioiodinated compound [^{125}I]**1** was performed on Beckman Gold HPLC system equipped with gradient solvent system, variable wavelength UV detector set at 254 nm, and a radiometric detector. Data were acquired and analyzed using the software (32 Karat®) provided by the vendor. [^{18}F]**4** was purified with a HPLC system that consisted of an Eldex Model 1SMP pump and a Knauer Model K-2501 UV–VIS detector (254 nm). Effluent from the UV–VIS detector was passed through a Carroll & Ramsey Associates Model 105S radiation detector. Chromatograms were recorded and analyzed using PeakSimple software (SRI Instruments). Quality control analysis of [^{18}F]**4** was performed on Beckman Gold HPLC system similar to that used for [^{125}I]**1**. LogP values were calculated for the final compounds based on their chemical structure using ACD/ChemSketch software (www.acdlabs.com).

Chemistry

***N*-(4-Butylphenyl)-3-(4-(2-iodophenyl)piperazine-1-carbonyl)-4-methylbenzenesulfonamide (1)**

To a stirred solution of 1-(2-iodophenyl)piperazine (0.065 g, 0.23 mmol) in dimethylformamide (8 mL) was added 1-ethyl-3-(3-dimethylaminopropyl)carbodiimide (EDC; 0.048 g, 0.26 mmol), N,N-diisopropylethylamine (0.18 mL, 0.78 mmol) at 0℃. After 5 min, hydroxybenzotriazole (HOBt; 0.040 g, 0.26 mmol) and 5-(*N*-(4-butylphenyl)sulfamoyl)-2-methylbenzoic acid (0.091 g, 0.23 mmol) were added and the resulting mixture was stirred at room temperature (RT) overnight.

The crude mixture was diluted with water (80 mL) and extracted with ethyl acetate (3 × 50 mL). The combined organic layers were washed with water followed by brine, and filtered over sodium sulfite. The filtrate was concentrated under reduced pressure, and subjected to purification using silica gel eluted with gradient mixtures of ethyl acetate (EtOAc) and hexanes (0→50%) to obtain **1** as an off-white solid (0.087 g, 62% yield), mp: 83-84 ℃. ^{1}H NMR ($CDCl_3$, 400 MHz): δ 7.86 (d, *J* = 7.6 Hz, 1H), 7.61 (m, 2H), 7.36 – 7.28 (m, 2H), 7.03 – 6.95 (m, 5H), 6.85 (t, *J* = 7.6 Hz, 1H), 4.06 (m, 2H), 3.27 (m, 2H), 3.05 (m, 2H), 2.79 (m, 2H), 2.47 (t, *J* = 7.2 Hz, 2H), 2.37 (s, 3H), 1.49 (m, 2H), 1.27 (m, 2H) 0.87 (t, *J* = 7.2 Hz, 3H). ^{13}C NMR ($CDCl_3$, 125 MHz) δ 168.25, 152.40, 140.45, 140.06, 137.12, 136.51, 133.81, 131.15, 129.34, 129.12, 127.63, 126.12, 124.97, 122.50, 121.17, 98.29, 52.74, 52.02, 47.28, 42.09, 34.91, 33.39, 28.00, 22.24, 19.26, 13.85. LC-MS (DART): *m/z* calcd. for $C_{28}H_{33}IN_3O_3S$ ($[M+H]^+$): 618.1287; observed: 618.1282

_N_-(4-Butylphenyl)-3-(4-(4-iodophenyl)piperazine-1-carbonyl)-4-methylbenzenesulfonamide (2)

To a stirred solution of 1-(4-iodophenyl)piperazine (0.40 g, 1.4 mmol) in dimethylformamide (40 mL) at 0℃ was added EDC (0.30 g, 1.58 mmol) and N, N-diisopropylethylamine (1.0 mL, 4.3 mmol). After 5 min, HOBt (0.25 g, 1.58 mmol) and 5-(*N*-(4-butylphenyl)sulfamoyl)-2-methylbenzoic acid (0.091 g, 0.23 mmol) were added and the mixture was allowed to warm to RT, and stirred for 36 h. The reaction mixture was then diluted with water and extracted with ethyl acetate (3 × 100 mL). The combined organic layers were washed with brine, dried with sodium sulfite and filtered. The filtrate was concentrated under reduced pressure, and the residue was purified using silica gel via flash column chromatography eluted with 45% EtOAc in hexanes. The fractions containing the title compound **2** were combined and evaporated to give the product as an off-white solid (0.62 g, 71% yield), mp: 154-156 ℃. ^{1}H NMR ($CDCl_3$, 400 MHz): δ 7.60 - 7.53 (m, 3H), 7.29 (m, 1H), 7.03 (d, *J* = 8.4, 2H), 6.95 (d, *J* = 8.4, 2H), 6.65 (m,

3H), 3.92 (m, 2H), 3.21 (m, 4H), 2.97 (m, 2H), 2.51 (t, *J* = 7.6 Hz, 2H), 2.35 (s, 3H) 1.52 (m, 2H), 1.28 (m, 2H), 0.87 (t, *J* = 7.2 Hz, 3H). ^{13}C NMR ($CDCl_3$, 125 MHz) δ 168.07, 150.25, 140.38, 140.06, 137.92, 137.12, 136.14, 133.82, 131.18, 129.09, 127.73, 124.87, 122.46, 118.71, 82.75, 49.46, 49.02, 46.48, 41.43, 34.93, 33.41, 22.24, 19.23, 13.85. LC-MS (DART): *m/z* calcd. for $C_{28}H_{33}IN_3O_3S$ ($[M+H]^+$): 618.1287; observed: 618.1294.

_N_-(4-Butylphenyl)-3-(4-(2-(2-fluoroethoxy)phenyl)piperazine-1-carbonyl)-4-methylbenzenesulfonamide (4)

Compound **4** was prepared a described for **1**, but using 1-(2-(2-fluoroethoxy)phenyl)piperazine (0.31 g, 1.38 mmol) and 5-(*N*-(4-butylphenyl)sulfamoyl)-2-methylbenzoic acid (0.5 g, 1.4 mmol) as starting materials to get 0.36 g of **4** as a white solid (47% yield), mp: 152-153 ℃. ^{1}H NMR ($CDCl_3$, 400 MHz): δ 7.63 (s, 1H), 7.58 (d, *J* = 7.6 Hz, 1H), 7.28 (d, *J* = 8.0 Hz, 1H), 7.03 – 6.87 (m, 8H), 6.64 (s, 1H), 4.77 (m, *J* = 47.2 Hz, 2H), 4.25 (m, *J* = 28.0 Hz, 2H), 3.97 (m, 2H), 3.27 (m, 2H), 3.15 (m, 2H), 2.92 (m, 2H), 2.48 (t, *J* = 7.2 Hz, 2H), 2.36 (s, 3H), 1.50 (m, 2H), 1.28 (m, 2H), 0.88 (t, *J* = 7.2 Hz, 3H). ^{13}C NMR ($CDCl_3$, 125 MHz) δ 168.14, 150.98, 141.06, 140.36, 139.91, 137.15, 136.55, 133.84, 131.02, 129.06, 127.58, 124.85, 123.45, 122.55, 122.11, 118.80, 113.60, 82.51, 81.15, 67.72, 67.57, 51.06, 50.36, 47.11, 41.96, 34.86, 33.37, 22.20, 19.20, 13.82. HRMS (DART): *m/z* calcd. for $C_{30}H_{37}FN_3O_4S$ ($[M+H]^+$): 554.2483; observed: 554.2481.

_N_-(4-Butylphenyl)-3-(4-(4-(2-fluoroethoxy)phenyl)piperazine-1-carbonyl)-4-methylbenzenesulfonamide (5)

Compound **5** was synthesized as described for **1**, but using 1-(4-(2-fluoroethoxy)phenyl)piperazine (0.14 g, 0.62 mmol) as the starting material. Purification of the crude mixture by flash column chromatography eluted with 0→60% EtOAc in hexanes provided the product **5** as an off-white solid in 40% yield (0.12 g), mp: 207-208 ℃. ^{1}H NMR ($CDCl_3$, 400

MHz): δ 7.61 – 7.58 (m, 2H), 7.27 (m, 1H), 7.04 – 6.87 (m, 8H), 4.74 (m, *J* = 47.6 Hz, 2H), 4.17 (m, *J* = 28.0 Hz, *J* = 4.0 Hz, 2H), 3.93 (m, 2H), 3.21 (m, 2H), 3.11 (m, 4H), 2.87 (m, 2H), 2.50 (t, *J* = 7.6 Hz, 2H), 2.35 (s, 3H), 1.29 (m, 2H), 0.88 (t, *J* = 7.2 Hz, 3H). ^{13}C NMR ($CDCl_3$, 125 MHz) δ 168.04, 153.23, 145.44, 140.36, 140.04, 137.11, 136.31, 133.86, 131.14, 129.09, 127.66, 124.88, 122.50, 118.89, 115.49, 82.66, 81.30, 67.67, 67.50, 51.23, 50.78, 46.87, 41.75, 34.92, 33.40, 22.23, 19.23, 13.83. LC-MS (DART): *m/z* calcd. for $C_{30}H_{37}FN_3O_4S$ ($[M+H]^+$): 554.2489; observed: 554.2489.

5-(Chlorosulfonyl)-2-iodobenzoic acid (8)

Chlorosulfonic acid (50 mL, 752 mmol) was cooled in an ice-NaCl bath under an atmosphere of argon. To this was added *o*-iodobenzoic acid (12.4 g, 50 mmol) in small portions over 5 min. The cooling bath was removed and the solution was allowed to warm to room temperature then heated overnight to 115℃ (oil bath temperature). T he reaction mixture was then cooled to RT and poured slowly over ice (~1L). The resulting precipitate was filtered, washed with water (2 × 200 mL) and dried. The solid residue was dissolved in EtOAc (400 mL) and the resulting amber solution was washed with brine (3 x 400 mL) then dried (Na_2SO_4). The drying agent was removed by filtration and the filtrate was concentrated to dryness under reduced pressure to afford the crude product (11 g, 63%) as a light orange solid. The crude product was used in the next step without further purification.

5-(*N*-(4-Butylphenyl)sulfamoyl)-2-iodobenzoic acid (9)

Solid 5-(chloromethylsulfonyl)-2-iodobenzenecarboxylic acid **8** (5.0 g, 11 mmol, 1.1 eq.) was added in one portion to a solution of 4-butylaniline (1.6 mL, 10 mmol) in pyridine (40 mL). The reaction was allowed to warm to RT as the cooling bath melted. Stirring was continued overnight (15 h) after which time overnight analysis of the reaction by TLC (50% EtOAc in hexanes) indicated complete consumption of the starting aniline. The reaction mixture was

diluted with CH_2Cl_2 (50 mL) and washed with 1N HCl (50 mL). The aqueous wash was extracted with CH_2Cl_2 (3 × 50 mL). The organic extracts were combined. Silica gel (~2 g) was added and the mixture was concentrated to dryness under reduced pressure. Flash column chromatography (RediSepRf SiO_2 (40 g), 100% CH_2Cl_2→5% MeOH in CH_2Cl_2) gave the product as a light brown brittle glass (0.713 g, 16%). Analysis of the material by LCMS showed a single peak at multiple wavelengths (210 nm, 221 nm, 254 nm and 280 nm). The area under those peaks corresponded to the expected mass-to-charge ratio (*m/z* = 476 [$(M+H)^+$] and 474 [$(M-H)^-$] and the material was used without further characterization.

_N_-(4-Butylphenyl)-4-iodo-3-(4-(2-methoxyphenyl)piperazine-1-carbonyl)benzenesulfonamide (3)

N,N-Diisopropylethylamine (1.1 mL, 6.3 mmol, 4 eq.) was added in one portion at room temperature to a (near) solution of the acid **9** (0.713 g, 1.6 mmol), HOBt (0.37 g, 2.3 mmol, 1.5 eq.), EDC (0.45 g, 2.3 mmol, 1.5 eq.) and 1-(-2-methoxyphenyl)piperazine (0.9 g, 3.9 mmol, 2.5 eq.) in anhydrous CH_2Cl_2 (25 mL). After 1 h, analysis of the reaction mixture by LCMS indicated complete consumption of starting acid. Silica gel (~3 g) was added and the mixture was concentrated under reduced pressure. Flash column chromatography (RediSepRf SiO_2 (40 g), 100% CH_2Cl_2 → 5% MeOH in CH_2Cl_2) gave the amide **3** as brownish-orange solid (0.6 g, 59%), mp: 87-89 ℃. ^{1}H NMR ($CDCl_3$, 400 MHz): δ 7.86 (d, *J* = 8.4 Hz, 1H), 7.62 (d, *J* = 2.4 Hz, 1H), 7.29 (dd, *J* = 2.4 H, 8.4 Hz, 1H), 7.03 (m, 3H), 6.96 - 6.86 (m, 5H), 6.80 (s, 1H), 3.96 (m, 2H), 3.86 (s, 3H), 3.31 (m, 1H), 3.17 (m, 2H), 3.08 (m, 2H), 2.89 (m, 1H), 2.49 (t, *J* = 7.2 Hz, 2H), 1.51 (m, *J* = 7.2 Hz, 2H), 1.29 (m, *J* = 7.2 Hz, 2H), 0.88 (t, *J* = 7.2 Hz, 3H). ^{13}C NMR ($CDCl_3$, 125 MHz) δ 167.89, 152.15, 149.56, 142.81, 140.70, 140.32, 140.05, 139.85, 136.16, 133.52, 129.19, 128.36, 126.44, 125.50, 123.68, 122.77, 121.03, 118.47, 111.33, 98.36, 55.39, 50.69, 50.16, 47.16, 42.09, 34.92, 33.38, 22.23, 13.84. ESI-MS: *m/z* calcd for $C_{28}H_{33}IN_3O_4S$ [$(M+H)^+$]: 634.1231; observed: 634.1227.

3-(4-Nitrophenyl)propan-1-ol (10a)

3-(4-Nitrophenyl)propionic acid (5.12 g, 26.20 mmol) in anhydrous THF (15 mL) was cooled in a NaCl bath, and a solution of BH_3 in THF (33 mL, 33 mmol, 1.3 eq.) was added dropwise over 5 minutes. Upon complete addition, the cooling bath was removed and the mixture was stirred for 2 h after which time analysis of the reaction by TLC (2% MeOH in CH_2Cl_2) indicated complete consumption of starting material. Silica gel (~8 g) was added and the mixture was concentrated to dryness under reduced pressure. Flash column chromatography (Redi*Sep*® Rf SiO_2 (80 g), 100% CH_2Cl_2 → 5% MeOH in CH_2Cl_2) gave the product as an orange oil (4.26 g, 90%). Analysis of the material by LCMS showed a single peak at multiple wavelengths (210 nm, 221 nm, 254 nm and 280 nm). The area under those peaks corresponded to the expected mass-to-charge ratio (m/z = 182 [$(M+H)^+$]) and the material was used without further characterization.

1-(3-Fluoropropyl)-4-nitrobenzene (11a)

A solution of 3-(4-nitrophenyl)propan-1-ol **10** (2.5 g, 13.8 mmol) in anhydrous CH_2Cl_2 (47 mL) was cooled in a dry ice/acetone bath. The solution was treated sequentially with 1,8-Diazabicyclo[5.4.0]undec-7-ene (DBU, 3.2 mL, 21 mmol, 1.5 eq.) and XtalFluor-M® (5 g, 21 mmol, 1.5 eq.). The mixture was stirred in the cold bath for 30 minutes then allowed to warm to room temperature overnight. The following morning, analysis of the reaction mixture by TLC (10% EtOAc in hexanes) indicated complete consumption of starting material. The reaction was quenched with saturated aqueous $NaHCO_3$ (50 mL) and the mixture was stirred for 30 min. Following phase separation, the aqueous phase was extracted with CH_2Cl_2 (2 × 25 mL). The combined organic extracts were dried ($MgSO_4$). The drying agent was removed by filtration. Silica gel (~5 g) was added and the filtrate was concentrated to dryness under reduced pressure. Flash column chromatography (Redi*Sep*® Rf SiO_2 (80 g), 100% hexanes → 10% EtOAc in hexanes) gave the product as a clear yellow oil (1.04 g, 41%). Analysis of the material by LCMS showed a single peak at multiple wavelengths (210 nm, 221 nm, 254 nm and 280

nm). The area under those peaks corresponded to the expected mass-to-charge ratio (*m/z* = 184 [$(M+H)^+$]) and the material was used without further characterization.

4-(3-Fluoropropyl)aniline (12a)

A solution of the nitro compound **11** (1.04 g, 5.7 mmol) and 10% Pd/C (0.25 g) in MeOH (15 mL) was stirred overnight under a balloon of H_2 after which time, analysis of the reaction mixture by TLC (10% EtOAc in hexanes) indicated complete consumption of starting material. The mixture was filtered through a pad of Celite. The pad was washed with MeOH (50 mL). Silica gel (~2 g) was added and the filtrate was concentrated to dryness under reduced pressure. Flash column chromatography (Redi*Sep*® Rf SiO_2 (40 g), 100% hexanes → 100% EtOAc in hexanes) gave the product as a clear amber liquid (0.62 g, 71%). Analysis of the material by LCMS showed a single peak at multiple wavelengths (210 nm, 221 nm, 254 nm and 280 nm). The area under those peaks corresponded to the expected mass-to-charge ratio (*m/z* = 154 [$(M+H)^+$]) and the material was used without further characterization.

5-(*N*-(4-(3-Fluoropropyl)phenyl)sulfamoyl)-2-methylbenzoic acid (13a)

Solid 5-(chloromethylsulfonyl)-2-methylbenzenecarboxylic acid (1.04 g, 4.43 mmol, 1.1 eq.) was added in one portion to an ice-bath cooled solution of 4-(3-fluoropropyl)aniline **12a** (0.617 g, 4.03 mmol) in pyridine (15 mL). The reaction was allowed to warm to room temperature as the cooling bath melted. Stirring was continued overnight (15 h) after which time analysis of the reaction by TLC (50% EtOAc in hexanes) indicated complete consumption of the starting aniline. The reaction mixture was diluted with CH_2Cl_2 (50 mL) and washed with 1N HCl (50 mL). The aqueous wash was extracted with CH_2Cl_2 (3 × 50 mL). The organic extracts were combined. Silica gel (~2 g) was added and the mixture was concentrated to dryness under reduced pressure. Flash column chromatography (Redi*Sep*® Rf SiO_2 (40 g), 100% hexanes → 100% EtOAc in hexanes) gave the product as an off-white solid (1.10 g, 74%). Analysis of the

material by LCMS showed a single peak at multiple wavelengths (210 nm, 221 nm, 254 nm and 280 nm). The area under those peaks corresponded to the expected mass-to-charge ratio (*m/z* = 368 [$(M+H)^+$] and 366 [$(M-H)^-$] and the material was used without further characterization.

_N_-(4-(3-Fluoropropyl)phenyl)-3-(4-(2-methoxyphenyl)piperazine-1-carbonyl)-4-methylbenzenesulfonamide (6)

N,N-Diisopropylethylamine (2.2 mL, 12.5 mmol, 4 eq.) was added in one portion at RT to a (near) solution of the benzoic acid derivative **13a** (1.10 g, 3.13 mmol), HOBt (0.73 g, 4.70 mmol, 1.5 eq.), EDC (0.9 g, 4.7 mmol, 1.5 eq.) and 1-(-2-methoxyphenyl)piperazine (1.78 g, 7.80 mmol, 2.5 eq.) in anhydrous CH_2Cl_2 (50 mL). After 1 h, analysis of the reaction mixture by LCMS indicated complete consumption of the starting material **13a**. Silica gel (~3 g) was added and the mixture was concentrated under reduced pressure. Flash column chromatography (Redi*Sep*® Rf SiO_2 (40 g), 100% CH_2Cl_2 → 50% EtOAc in CH_2Cl_2) gave the amide compound **6** as an off-white solid (1.40 g, 85%), mp: 198-199 ℃ . ^{1}H NMR ($CDCl_3$, 400 MHz): δ 7.66 (s, 1H), 7.59 (d, *J* = 8.0 Hz, 1H), 7.28 (m, 3H), 7.05 - 6.89 (m, 8H), 4.45 (t, *J* = 5.6 Hz, 1H), 4.33 (t, *J* = 5.6 Hz, 1H), 3.96 (m, 2H), 3.87 (s, 3H), 3.29 (t, *J* = 4.8 Hz, 2H), 3.11 (m, 2H), 2.90 (m, 2H), 2.36 (s, 3H), 1.95 (m, 1H), 1.91 (m, 1H), 1.66 (s, 1H). ^{13}C NMR ($CDCl_3$, 125 MHz) δ 168.11, 152.15, 140.29, 139.98, 138.39, 137.14, 136.55, 134.41, 131.06, 129.18, 127.55, 124.88, 123.68, 122.43, 121.03, 118.45, 111.35, 83.51, 82.20, 55.38, 51.03, 50.47, 47.10, 41.94, 31.84, 31.68, 30.59, 30.56, 19.21. ESI-MS: *m/z* calcd. for $C_{28}H_{33}FN_3O_4S$ [$(M+H)^+$]: 526.2170; observed: 526.2169.

_N_-(4-(4-Fluorobutyl)phenyl)-3-(4-(2-methoxyphenyl)piperazine-1-carbonyl)-4-methylbenzenesulfonamide (7)

N,N-Diisopropylethylamine (1.8 mL, 10.5 mmol, 4 eq.) was added in one portion at RT to a (near) solution of the acid **13b** (1.0 g, 2.62 mmol), HOBt (0.61 g, 3.90 mmol, 1.5 eq.), EDC (0.75

g, 3.90 mmol, 1.5 eq.) and 1-(-2-methoxyphenyl)piperazine (1.25 g, 6.60 mmol, 2.5 eq.) in anhydrous CH_2Cl_2 (50 mL). After 1 h, analysis of the reaction mixture by LCMS indicated complete consumption of the starting acid. Silica gel (~3 g) was added and the mixture was concentrated under reduced pressure. Flash column chromatography (RediSepRf SiO_2 (40 g), 100% CH_2Cl_2 → 50% EtOAc in CH_2Cl_2) gave the amide **7** as an off white solid (1.1 g, 78%), mp: 160-161 ℃. 1H NMR ($CDCl_3$, 400 MHz) δ 7.62 (s, 1H), 7.58 (d, *J* = 8.0 Hz, 1H), 7.25 (m, 3H), 7.05 – 6.86 (m, 8H), 4.45 (t, *J* = 5.6 Hz, 1H), 4.33 (t, *J* = 5.6 Hz, 1H), 3.97 (m, 2H), 3.85 (s, 3H), 3.26 (t, *J* = 4.8 Hz, 2H), 3.10 (m, 2H), 2.87 (m, 2H), 2.34 (s, 3H), 1.66 – 1.62 (m, 5H). ^{13}C NMR ($CDCl_3$, 125 MHz) δ 168.11, 152.16, 140.31, 139.97, 139.34, 137.13, 136.53, 134.21, 131.04, 129.07, 127.56, 124.87, 123.67, 122.45, 121.02, 118.46, 111.34, 84.43, 83.12, 55.38, 51.01, 50.50, 47.10, 41.94, 34.64, 29.86, 29.70, 26.78, 26.75, 19.21. ESI-MS: *m/z* calcd for $C_{29}H_{35}FN_3O_4S$ [$(M+H)^+$]: 540.2327; observed: 540.2329.

3-(4-(2-Bromophenyl)piperazine-1-carbonyl)-*N*-(4-butylphenyl)-4-methylbenzenesulfonamide (14)

This was synthesized as described for compound **1** using 1-(2-bromophenyl)piperazine (0.17 g, 0.70 mmol) and 5-(*N*-(4-butylphenyl)sulfamoyl)-2-methylbenzoic acid **8** (0.25 g, 0.70 mmol) as starting materials. Purification of the crude material by flash column chromatography (0→50% EtOAc in hexanes) yielded the bromo precursor **14** as an off-white solid (0.31 g, 77%), mp: 86-87 ℃. ^{1}H NMR ($CDCl_3$, 400 MHz): δ 7.61 – 7.57 (m, 2H), 7.31 – 7.21 (m, 2H), 7.1 – 6.92 (m, 6H), 6.62 (s, 1H), 3.98 (m, 2H), 3.25 (m, 2H), 3.09 (m, 2H), 2.84 (m, 2H), 2.47 (t, *J* = 8.0 Hz, 2H) 2.37 (s, 3H), 1.51 (m, 2H), 1.28 (m, 2H), 0.87 (t, *J* = 7.2 Hz, 3H). ^{13}C NMR ($CDCl_3$, 125 MHz) δ 168.25, 149.63, 140.40, 139.99, 137.10, 136.45, 133.85, 131.14, 129.09, 128.39, 127.64, 125.10, 124.96, 122.48, 121.11, 119.98, 52.06, 51.37, 47.16, 41.99, 34.90, 33.38, 22.23, 19.24, 13.83. LC-MS (DART): *m/z* calcd. for $C_{28}H_{33}BrN_3O_3S$ [$(M+H)^+$]: 572.1406; observed: 572.1398.

_N_-(4-Butylphenyl)-3-(4-(2-hydroxyphenyl)piperazine-1-carbonyl)-4-methylbenzenesulfonamide (15)

This was synthesized as described for compound **1**, but starting from 2-(piperazin-1-yl)phenol (0.15 g, 0.84 mmol) and 5-(*N*-(4-butylphenyl)sulfamoyl)-2-methylbenzoic acid (0.3 g, 0.84 mmol). Purification of the crude mixture by flash column chromatography (0→50% EtOAc in hexanes) gave the phenol precursor **15** as an off-white solid (0.23 g, 54%), mp: 158-160 ℃. ^{1}H NMR ($CDCl_3$, 400 MHz): δ 7.63 – 7.57 (m, 2H) 7.31 (d, *J* = 8.4 Hz, 1H) 7.17 – 6.87 (m, 8H), 6.63 (s, 1H) 3.95 (m, 2H), 3.23 (m, 2H), 2.94 (m, 2H), 2.68 (m, 2H), 2.46 (t, *J* = 7.6 Hz, 2H), 2.38 (s, 3H), 1.49 (m, 2H), 1.27 (m, 2H), 0.87 (t, *J* = 7.2 Hz, 3H). ^{13}C NMR ($CDCl_3$, 125 MHz) δ 168.22, 151.09, 140.44, 140.01, 137.95, 137.12, 136.24, 133.80, 131.21, 129.11, 127.73, 126.94, 124.93, 122.43, 121.29, 120.28, 114.54, 52.68, 52.22, 47.37, 42.25, 34.84, 33.37, 22.20, 19.25, 13.81. LC-MS: *m/z* calcd. for $C_{28}H_{34}N_3O_4S$ ($[M+H]^+$): 508.2270; observed: 508.2269.

Radiochemistry

_N_-(4-Butylphenyl)-3-(4-(2-[^{125}I]iodophenyl)piperazine-1-carbonyl)-4-methylbenzenesulfonamide ([^{125}I]1)

To a solution of the bromo precursor **14** in ethanol (0.2 mg in 20 µL; 0.35 µmol) in a 0.2 mL Reacti-Vial™ were added 80 µL of a 10 mg/mL solution of gentisic acid (ethanol/ H_2O, 75/25, v/v) and 18 µL of 0.013 M $CuSO_4$ (H_2O). The reaction mixture was purged with argon for 5 min followed by the addition of [^{125}I]NaI (3-13 µL, 46-145 MBq). The reaction vial was tightly closed using a screw cap with septum (PTFE/silicone disc) and was heated at 140℃ for 1 h in an oil bath. The mixture was cooled to RT, and was purified using RP-HPLC on an XTerra® C_{18} column (5 µm, 4.6 mm × 250 mm; Waters) eluted with 60% acetonitrile in water with 0.1% TFA, at a flow rate of 1 mL/min. The HPLC peak corresponding to [^{125}I]**1** was collected (t_R = 26-28

min), diluted to 10 mL with water and loaded onto a pre-conditioned Sep-Pak® SPE cartridge (C_{18}, Waters). After rinsing the cartridge with water (5 mL), the labeled product was eluted with ethanol and 50-µL fractions were collected. Most of the activity was eluted in fractions 3-6, which were used for biological experiments. The identity confirmation of the purified [^{125}I]**1** was achieved by co-injection with the unlabeled analog **1** on the HPLC system as described for the purification.

N-(4-Butylphenyl)-3-(4-(2-(2-[^{18}F]fluoroethoxy)phenyl)piperazine-1-carbonyl)-4-methylbenzenesulfonamide ([^{18}F]4)

[^{18}F]Fluoride, obtained on a QMA® cartridge, was eluted into a conical reaction vial with a Kryptofix (37.2 mg/mL) and K_2CO_3 (3.3 mg/mL) solution in acetonitrile/water (0.75 mL, 95/5, v/v). Removal of solvents and further drying of the activity was achieved by heating the reaction vial at 100℃ and by azeotropic distillation with a cetonitrile (3 × 0.75 mL) under a stream of N_2. The dried activity was allowed to cool to RT, and a solution of 2-bromoethyl triflate in *O*-dichlorobenzene was added to the reaction vessel (5 µL in 0.7 mL). The mixture was then heated at 120℃ while bubbling with N_2, and the resulting [^{18}F]fluoroethyl bromide ([^{18}F]FEtBr) along with the N_2 sweep gas was passed through a C_{18} Sep-Pak before collecting the activity in a conical reaction vial that contained the phenol precursor **15** (0.5 mg) and Cs_2CO_3 in DMF (0.25 mL). Upon completion of the distillation and/or collecting sufficient activity (~20 min), the reaction vial was tightly closed and the labeling mixture was heated at 120℃ for 15 min for the ^{18}F-fluoroethylation reaction. The crude mixture was diluted with water (1.5 mL) and injected onto an XBridge® C_{18} column (5 µm, 4.6 × 150 mm) for purification. The product was eluted with 45% EtOH in 0.05 M sodium acetate buffer (pH 5.5) at a flowrate of 1 mL/min (t_R = 18.0 min). The identity of the purified [^{18}F]**4** was confirmed by co-elution with nonradioactive analog **4** on a RP-HPLC system that consisted of an XTerra® C_{18} column (5 µm, 4.6 × 250 mm) eluted with gradient mixtures of acetonitrile (A) and water (B) containing 0.1% TFA in both the solvents. The

% of acetonitrile was kept constant at 5% for the first 5 min and was then increased to 90 % over 30 min at a flow rate of 1 mL/min. The UV absorbance was measured at 254 nm. [^{18}F]**4** eluted with a retention time of 27.2 min compared to 27.0 min for the cold analog **4**.

Mutant IDH1 Inhibition Assays

The inhibitory efficiency of the synthesized nonradioactive analogs against mutant IDH1 was evaluated using purified IDH1-R132H enzyme in standard 384-well plates. Recombinant IDH1-R132H protein was derived as described previously [10] by expression with a C-terminal 6×His Tag in E. coli followed by purification using a Ni-NTA spin column (Qiagen, Hilden, Germany). For inhibition assays, serially-diluted solutions of nonradioactive test compounds in DMSO (1 µL) were added to wells that were pre-loaded with 25 µL of substrate mixture consisting of α-ketoglutarate (2 mM) and NADPH (8 µM). After centrifugation of the plate at 300*g* for 3 min, a diluted solution of IDH1-R132H enzyme (25 µL; 7.5 ng/µL) was added to the reaction mixture. After a second centrifugation, the mixture was incubated at RT for 50 min followed by the addition of developer mixture (25 µL) containing resazurin (30 µM) and diaphorase enzyme (36 µg/mL). The mixture was incubated for 5 min, and the fluorescence intensity in reaction mixtures was measured by reading the plates on a POLARstar Optima plate reader (BMG Labtech, Germany) using 544 nm and 590 nm as excitation and emission wavelengths, respectively. It should be noted that the fluorescence reaction is enabled by the conversion of resazurin to a highly fluorescent resorufin by the diaphorase enzyme, and the signal intensity is proportional to the unconsumed NADPH present in the reaction mixture. Efficient inhibition of the mutant IDH1 by the test compounds results in a high fluorescence signal due to the presence of high NADPH in the reaction mixture, whereas low fluorescence in wells is an indicative of uninhibited reactions.

Functional Inhibition Assay

The ability of compounds **1** and **4** to inhibit the neomorphic activity of the mutant, IDH1-R132H, was evaluated using isogenic anaplastic astrocytoma cell lines carrying a native IDH1-R132H mutation or WT-IDH1. The IDH1-R132H-mutated astrocytoma cell line was a subclone derived from a WHO grade III anaplastic astrocytoma; this line was described previously [19]. The isogenic WT-IDH1 cell line was a sister subclone derived at the same time from the same astrocytoma tumor cells. The WT-IDH1 cell line had lost the IDH1-R132H allele during cell line passage and retained only the IDH1-WT allele. Sanger sequencing was used to confirm that only the wild type IDH1 sequence and no mutant IDH1-R132H sequence was retained in the WT-IDH1 cell line. Likewise, Sanger sequencing was used to confirm that the WT-IDH1 cell line retained all other known genetic alterations found in the original tumor and in the isogenic IDH1-R132H cell line, including TP53 (TP53 p.G245V) and ATRX (ATRX p.R781X) mutations. The AmpFlSTR® Identifiler® Direct PCR Amplification Kit (Applied Biosystems) was used to confirm that the D2S1338 locus at chromosome 2q35 near the IDH1 locus was reduced to one marker for the WT-IDH1 cell line, consistent with loss of heterozygosity at the IDH1 locus for the WT-IDH1 subline.

For inhibition assays, cells were seeded in duplicate in standard 12-well plates at a density of 30,000 per well. Upon reaching full confluency, the incubation media was replaced with fresh media containing the unlabeled compounds **1** or **4** (50 μM, n=2/experiment). The drug-containing media was prepared from 20 mM stock solutions of compounds (DMSO). Cells were then incubated under standard cell culture conditions and aliquots (0.1 mL) of supernatant were removed at 4 and 8 h after incubation. The samples were stored at -80^{o}C until analysis by LC-MS/MS. The concentration of D-2-HG in the samples was measured by LC-MS/MS as described before [14]. The WT-IDH1 cell line and IDH1-132H cells that were treated with vehicle alone served as controls.

Cell Uptake Studies

Cell uptake of the labeled inhibitors was evaluated using the aforementioned IDH1 mutant and WT-IDH1 astrocytoma cell lines. Approximately 24 h before the uptake studies, cells were plated in standard 24-well plates at a density of 20,000 – 30,000 per well in 0.5 mL cell culture media. On the day of experiment, the media was removed, cells were washed with 0.5 mL PBS, and incubated with the labeled inhibitor [^{125}I]**1** (~3.7 kBq/well) in 0.25 mL of cell culture media. Cells were incubated at 37℃ and 5% CO_2 atmosphere for 0.25 – 4 h. After incubation, the media was removed, cells were washed with ice cold PBS (3 × 0.3 mL) and treated with Promega Luciferase Cell Culture Lysis Reagent (0.2 mL) for 5 min at RT. The cell lysate was collected into Eppendorf tubes, and the wells were rinsed with equal volume of PBS (0.2 mL). The lysate and the PBS rinse were combined and measured for radioactivity in an automated gamma counter (Wallac Wizard, Perkin Elmer). The radioactivity in cell supernatants as well as wash fractions was also measured, and the cell uptake was calculated as % of the incubation dose for each well. For co-incubation experiments, cells were incubated with [^{125}I]**1** and varying concentrations of unlabeled **1** (0 – 100 µM) for 3 h, and the uptake was determined as described for the tracer-alone incubation experiments. The effect of varying concentrations of FBS in the incubation media was evaluated by incubating of cells with [^{125}I]**1** in media containing 0.1% or 1% FBS for comparison to the 10% FBS in the full growth media. For the co-incubation experiments and FBS experiments, the uptake was normalized to protein levels in wells and the results are presented as % uptake/mg protein.

Tissue Distribution Studies

Tissue distribution studies were conducted for [^{125}I]**1** using 6-week old BALB/C mice (NCI, Frederick). The animal experiments were conducted in accordance with Institutional Animal Care and Use Committee (IACUC) guidelines and an approved animal protocol. Animals were injected via the tail vein with about 185 kBq of [^{125}I]**1** in PBS (0.1 mL) containing 0.1% BSA and were euthanized by isoflurane overdose at 5 min, 1 h, 2 h or 4 h after injection (n = 5 mice/time

point). Blood and vital organs were collected, weighed and measured for radioactivity in an automated gamma counter. The radioactivity uptake and distribution in different organs and tissues was calculated as % injected dose (%ID) and %ID per gram tissue (%ID/g).

Acknowledgments

The authors thank Genglin Jin for derivation of cell lines used in this work, Dr. Anthony Ribeiro for acquiring the ^{13}C NMR spectra, Dr. Gerald Bida for help with the ^{18}F-labeling experiments, Dr. Ganesan Vaidyanathan for helpful discussions on radioiodination of **1**, and Dr. Xiao-Guang Zhao for carrying out the biodistribution experiments. This work was supported by a research grant from the Southeastern Brain Tumor Foundation (SBTF) and NIH grant CA182025.

Supplementary Data

Supplementary data associated with this article can be found in the online version.

References

[1] Q. Lu, K. I. Minard, L. McAlister-Henn, Dual compartmental localization and function of mammalian NADP+-specific isocitrate dehydrogenase in yeast, Arch. Biochem. Biophys. 472 (2008) 17-25.

[2] H. Yang, D. Ye, K.-L Guan, Y. Xiong, IDH1 and IDH2 mutations in tumorigenesis: mechanistic insights and clinical perspectives, Clin. Cancer Res. 18 (2012) 5562-5571.

[3] D. W. Parsons, S. Jones, X. S. Zhang, J. C. H. Lin, R. J. Leary, P. Angenendt, P. Mankoo, H. Carter, I. M. Siu, G. L. Gallia, A. Olivi, R. McLendon, B. A. Rasheed, S. T. Keir, Y. Nikolskaya, D. A. Nikolsky, H. Busam, L. A. Tekleab, J. Diaz, D. R. Smith, R. L. Strausberg, S. K. N. Marie, S. M. O. Shinjo, H. Yan, G. J. Riggins, D. D. Bigner, R. Karchin, N. Papadopoulos, G. Parmigiani, B. Vogelstein, V. E. Velculescu, K. W. Kinzler, An integrated genomic analysis of human glioblastoma Multiforme, Science 321 (2008) 1807-1812.

[4] H. Yan, D. W. Parsons, G. L. Jin, R. McLendon, B. A. Rasheed, W. S. Yuan, I. Kos, I. Batinic-Haberle, S. Jones, G. J. Riggins, H. Friedman, A. Friedman, D. Reardon, J. Herndon, K. W. Kinzler, V. E. Velculescu, B. Vogelstein, D. D. Bigner, IDH1 and IDH2 mutations in gliomas, N. Engl. J. Med. 360 (2009) 765-773.

[5] R. A. Cairns, T. W. Mak, Oncogenic isocitrate dehydrogenase mutations: mechanisms, models, and clinical opportunities, Cancer Discov. 3 (2013) 730-741.

[6] Cancer Genome Atlas Research Network, Comprehensive, integrative genomic analysis of diffuse lower-grade gliomas, N. Engl. J. Med. 372 (2015) 2481-2498.

[7] P. Zou, H. Xu, P. Chen, Q. Yan, L. Zhao, P. Zhao, A. Gu, IDH1/IDH2 mutations define the prognosis and molecular profiles of patients with gliomas: a meta-analysis, PLoS One 8, (2013) e68782.

[8] M. S. Waitkus, B. H. Diplas, H. Yan, Isocitrate dehydrogenase mutations in gliomas, Neuro Oncol. 18 (2016) 16-26.

[9] T. Watanabe, S. Nobusawa, P. Kleihues, H. Ohgaki, IDH1 mutations are early events in the development of astrocytomas and oligodendrogliomas, Am. J. Pathol. 174 (2009) 1149-1153.

[10] L. Dang, D. W. White, S. Gross, B. D. Bennett, M. A. Bittinger, E. M. Driggers, V. R. Fantin, H. G. Jang, S. Jin, M. C. Keenan, K. M. Marks, R. M. Prins, P. S. Ward, K. E. Yen, L. M. Liau, J. D. Rabinowitz, L. C. Cantley, C. B. Thompson, M. G. Vander Heiden, S. M. Su, Cancer-associated IDH1 mutations produce 2-hydroxyglutarate, Nature 462 (2009) 739-744.

[11] R. Chowdhury, K. K. Yeoh, Y.-M. Tian, L. Hillringhaus, E. A. Bagg, N. R. Rose, I. K. H. Leung, X. S. Li, E. C. Y. Woon, M. Yang, M. A. McDonough, O. N. King, I. J. Clifton, R. J. Klose, T. D. W. Claridge, P. J. Ratcliffe, C. J. Schofield, A. Kawamura, The oncometabolite 2-hydroxyglutarate inhibits histone lysine demethylases, Embo Reports 12 (2011) 463-469.

[12] M. E. Figueroa, O. Abdel-Wahab, C. Lu, P. S. Ward, J. Patel, A. Shih, Y. Li, N. Bhagwat, A. Vasanthakumar, H. F. Fernandez, M. S. Tallman, Z. Sun, K. Wolniak, J. K. Peeters, W. Liu, S. E. Choe, V. R. Fantin, E. Paietta, B. Lowenberg, J. D. Licht, L. A. Godley, R. Delwel, P. J. M. Valk, C. B. Thompson, R. L. Levine, A. Melnick, Leukemic IDH1 and IDH2 mutations result in a hypermethylation phenotype, disrupt TET2 function, and impair hematopoietic differentiation, Cancer Cell 18 (2010) 553-567.

[13] W. Xu, H. Yang, Y. Liu, Y. Yang, P. Wang, S.-H. Kim, S. Ito, C. Yang, P. Wang, M.-T. Xiao, L.-X. Liu, W.-Q. Jiang, J. Liu, J.-Y. Zhang, B. Wang, S. Frye, Y. Zhang, Y.-H. Xu, Q.-Y. Lei, K.-L. Guan, S.-M. Zhao, Y. Xiong, Oncometabolite 2-hydroxyglutarate is a competitive inhibitor of alpha-ketoglutarate-dependent dioxygenases, Cancer Cell 19 (2011) 17-30.

[14] C. G. Duncan, B. G. Barwick, G. Jin, C. Rago, P. Kapoor-Vazirani, D. R. Powell, J. T. Chi, D. D. Bigner, P. M. Vertino, H. Yan, A heterozygous IDH1R132H/WT mutation induces genome-wide alterations in DNA methylation, Genes Dev. 22 (2012) 2339-2355.

[15] Z. J. Reitman, G. Jin, E. D. Karoly, I. Spasojevic, J. Yang, K. W. Kinzler, Y. He, D. D. Bigner, B. Vogelstein, H. Yan, Profiling the effects of isocitrate dehydrogenase 1 and 2 mutations on the cellular metabolome, Proc. Natl. Acad. Sci. U.S.A. 108 (2011) 3270-3275.

[16] H. Wen, H. R. Cho, T. Yun, H. Kim,, C. K. Park, S. H. Lee, S. H. Choi, S. Park, Metabolomic comparison between cells over-expressing isocitrate dehydrogenase 1 and 2 mutants and the effects of an inhibitor on the metabolism, J. Neurochem. 132 (2015) 183-193.

[17] F. G. Salituro, J. O. Saunders, Therapeutically active compounds for use in the treatment of cancer characterized as having an IDH mutation, Patent WO 2011/072174 A1 (2011).

[18] L. Bhat, P. P. Mohapatra, S. R. Bhat, Compositions, synthesis, and methods of using quinolinone based atypical antipsychotic agents, Patent US 2008/0293736 A1 (2008).

[19] G. Jin, Z. J. Reitman, C. G. Duncan, I. Spasojevic, D. M. Gooden, B. A. Rasheed, R. Yang, G. Y. Lopez, Y. He, R. E. McLendon, D. D. Bigner, Hai Yan, Disruption of wild-type IDH1 suppresses D-2-hydroxyglutarate production in IDH1-mutated gliomas, Cancer Res. 73 (2013) 496-501.

[20] M. I. Davis, S. Gross, M. Shen, K. S. Straley, R. Pragani, W. A. Lea, J. Popovici-Muller, B. DeLaBarre, E. Artin, N. Thorne, D. S. Auld, Z. Li, L. Dang, M. B. Boxer, A. Simeonov, Biochemical, cellular, and biophysical characterization of a potent inhibitor of mutant isocitrate dehydrogenase IDH1, J. Biol. Chem. 289 (2014) 13717-13725.

[21] J. Popovici-Muller, J. O. Saunders, F. G. Salituro, J. M. Travins, S. Yan, F. Zhao, S. Gross, L. Dang, K. E. Yen, H. Yang, K. S. Straley, S. Jin, K. Kunii, V. R. Fantin, S. Zhang, Q. Pan, D. Shi, S. A. Biller, S. M. Su, Discovery of the first potent inhibitors of mutant IDH1 that lower tumor 2-HG in vivo, ACS Med. Chem. Lett. 3 (2012) 850-855.

[22] M. Ceusters, D. Tourwe, J. Callaerts, J. Mertens, A. Peter, New single-step radioiodination technique for peptides: Cu(I)-catalyzed nucleophilic nonisotopic displacement reaction.

Synthesis of radioiodinated deltorphin and dermorphin analogues, J. Org. Chem. 60 (1995) 8324-8326.

[23] S. K. Chitneni, C. M. Deroose, J. Balzarini, R. Gijsbers, S. J. L. Celen, T. J. de Groot, Z. Debyser, L. Mortelmans, A. M. Verbruggen, G. M. Bormans, Synthesis and preliminary evaluation of ^{18}F or ^{11}C-labeled bicyclic nucleoside analogues as potential probes for imaging varicella-zoster virus thymidine kinase gene expression using positron emission tomography, J. Med. Chem. 50 (2007) 1041-1049.

[24] Z. Su, F. Roncaroli, P. F. Durrenberger, D. J. Coope, K. Karabatsou, R. Hinz, G. Thompson, F. E. Turkheimer, K. Janczar, D. Du Plessis, A. Brodbelt, A. Jackson, A. Gerhard, K. Herholz, The 18-kDa mitochondrial translocator protein in human gliomas: an ^{11}C-(*R*)PK11195 PET imaging and neuropathology study, J. Nucl. Med. 56 (2015) 512-517.

[25] M. Bruehlmeier, U. Roelcke, P. A. Schubiger, S. M. Ametamey, Assessment of hypoxia and perfusion in human brain tumors using PET with ^{18}F-fluoromisonidazole and ^{15}O-H_2O, J. Nucl. Med. 45 (2004) 1851-1859.

[26] M. M. Hann, G. M. Keserü, Finding the sweet spot: the role of nature and nurture in medicinal chemistry. Nat. Rev. Drug Discov. 11 (2012) 355-365.

[27] D. Rohle, J. Popovici-Muller, N. Palaskas, S. Turcan, C. Grommes, C. Campos, J. Tsoi, O. Clark, B. Oldrini, E. Komisopoulou, K. Kunii, A. Pedraza, S. Schalm, L. Silverman, A. Miller, F. Wang, H. Yang, Y. Chen, A. Kernytsky, M. K. Rosenblum, W. Liu, S. A. Biller, S. M. Su, C. W. Brennan, T. A. Chan, T. G. Graeber, K. E. Yen, I. K. Mellinghoff, An inhibitor of mutant IDH1 delays growth and promotes differentiation of glioma cells, Science 340 (2013) 626-630.

Figure Legends

Figure 1. Chemical structure of the reference mutant IDH1 inhibitor **A**.

Figure 2. Chemical structures, inhibitory potency and the maximal inhibition values (%) for the synthesized mutant IDH1-R132H inhibitors and the reference analog **A**. Inhibitory efficiency is presented as mean±SD (n = 3-4) for each of the compounds.

Figure 3. Determination of inhibitory potency for the nonradioactive analogs using purified IDH1-R132H enzyme. The IC_{50} values are shown in parenthesis for the corresponding compounds. The *para*-fluoroethoxy analog **5** displayed a partial inhibitory response with a mean inhibition efficiency of 26.4%.

Figure 4. Inhibition of the mutant IDH1 activity (2-HG production) by the nonradioactive analogs **1** and **4** (50 µM) at 8 h after incubation in IDH1 mutated astrocytoma cells. The 2-HG levels in the WT-IDH1 control cells are also shown in the Figure for comparison.

Figure 5. Identity conformation of the HPLC-purified radiolabeled inhibitors [^{125}I]**1** (A) and [^{18}F]**4** (B) by co-elution with the corresponding nonradioactive analog on an analytical HPLC.

Figure 6. Tissue distribution data for the radioiodinated inhibitor [^{125}I]**1** in in BALB/C mice at 5 min – 4 h after injection. Data is shown as %ID/g values for different organs (n=5 animals/time point).

Figure 7. Uptake of [^{125}I]**1** in astrocytoma cells that are positive for an IDH1-R132H mutation, and in WT-IDH1 cells. (A) Percent added activity taken up in mutant IDH1 and WT-IDH1

astrocytoma cells at 0.25 – 4 h after incubation. (B) Uptake of [^{125}I]**1** in the presence of increasing concentrations of the unlabeled **1** in the incubation media (0.1 – 100 µM, 3 h). (C) Effect of varying concentrations of FBS (%) in the incubation media on [^{125}I]**1** uptake at 3 h after incubation.

Scheme Legends

Scheme 1. General synthesis route for preparation of the *ortho*- and *para*-substituted inhibitors **1**, **2**, **4** and **5**.

Scheme 2. Synthesis scheme for the iodo analog **3**.

Scheme 3. Synthesis scheme for the fluoropropyl- and fluorobutyl phenyl sulfonamide analogs **6** and **7**.

Scheme 4. Radiosynthesis of [^{125}I]**1** using the bromo precursor **14**.

Scheme 5. Radiosynthesis of [^{18}F]**4** using [^{18}F]fluoroethyl bromide and the phenol precursor **15**.

Figure 1

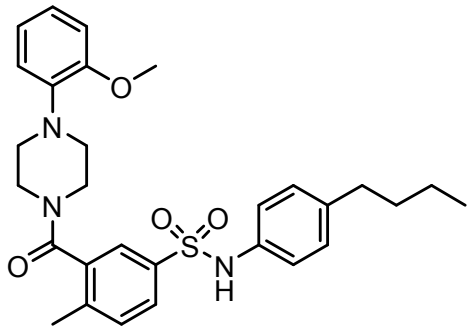

A

Figure 2

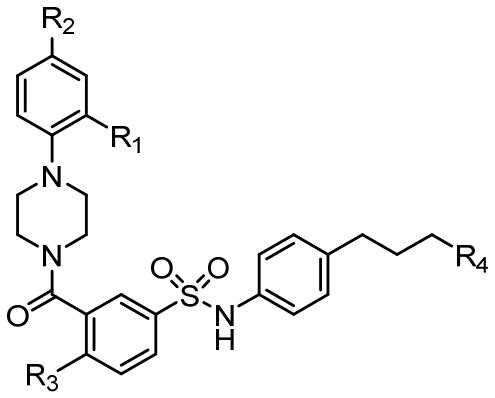

Compound	R_1	R_2	R_3	R_4	IC_{50} (μM)	Inhibition Efficiency (%)
A	OCH_3	H	CH_3	CH_3	2.2	102.6 ± 10.6
1	I	H	CH_3	CH_3	1.7	106.7 ± 11.6
2	H	I	CH_3	CH_3	*n.a.*	4.1
3	OCH_3	H	I	CH_3	*n.t.*	*n.t*
4	OCH_2CH_2F	H	CH_3	CH_3	2.3*	106.6 ± 18.3*
5	H	OCH_2CH_2F	CH_3	CH_3	1.2	26.4 ± 13.6
6	OCH_3	H	CH_3	F	2.7	98.7 ± 18.0
7	OCH_3	H	CH_3	CH_2F	2.4	81.3 ± 17.1

n.a. - not active; n.t. - not tested

**mean value derived from three separate experiments (e.g. see Fig. 3)*

Figure 3

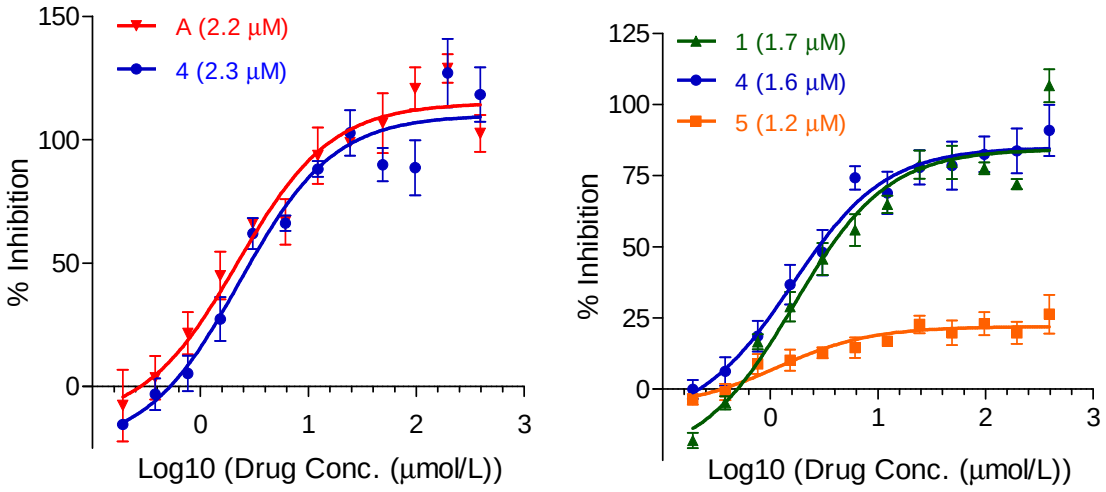
150
100
50
0
% Inhibition
A (2.2 µM)
4 (2.3 µM)
0
1
2
3
Log10 (Drug Conc. (µmol/L))
125
100
75
50
25
0
% Inhibition
1 (1.7 µM)
4 (1.6 µM)
5 (1.2 µM)
0
1
2
3
Log10 (Drug Conc. (µmol/L))

Figure 4

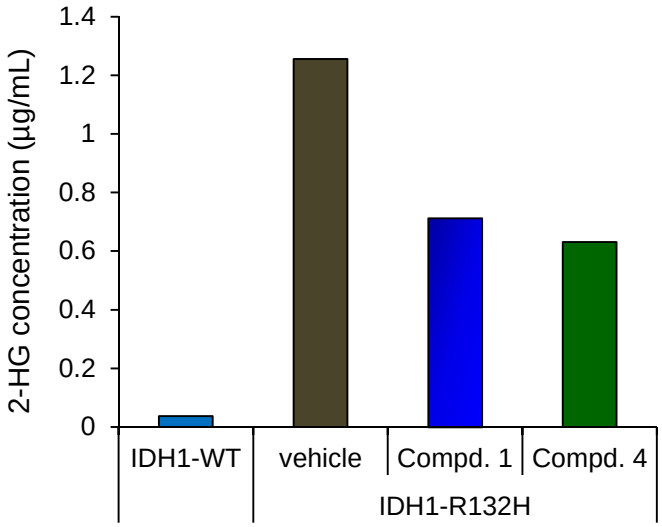
2-HG concentration (µg/mL)
1.4
1.2
1
0.8
0.6
0.4
0.2
0
IDH1-WT
vehicle
Compd. 1
Compd. 4
IDH1-R132H

Figure 5

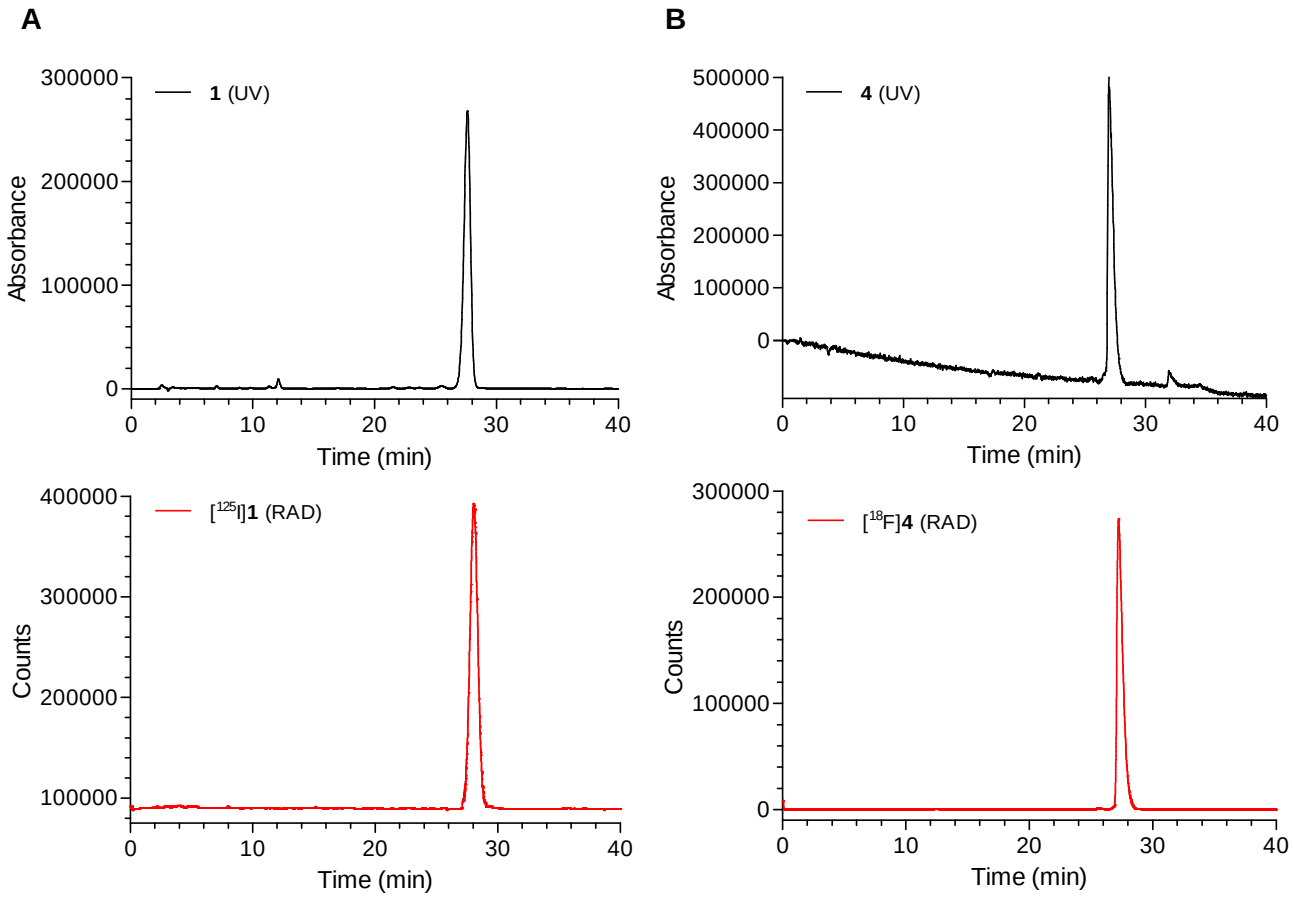

Figure 6

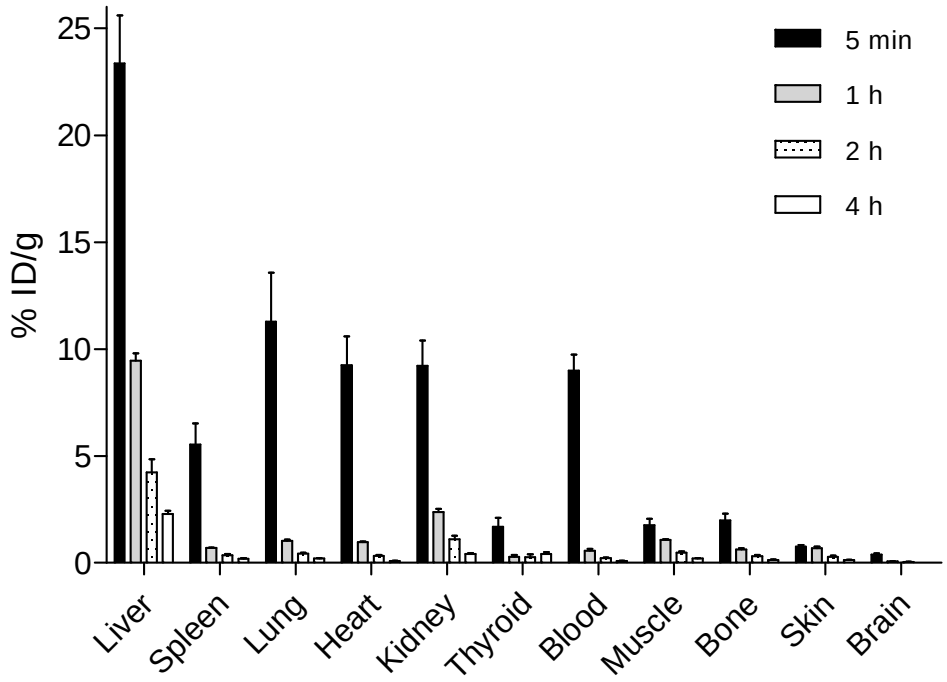
25
20
15
10
5
0
% ID/g
5 min
1 h
2 h
4 h
Liver
Spleen
Lung
Heart
Kidney
Thyroid
Blood
Muscle
Bone
Skin
Brain

Figure 7

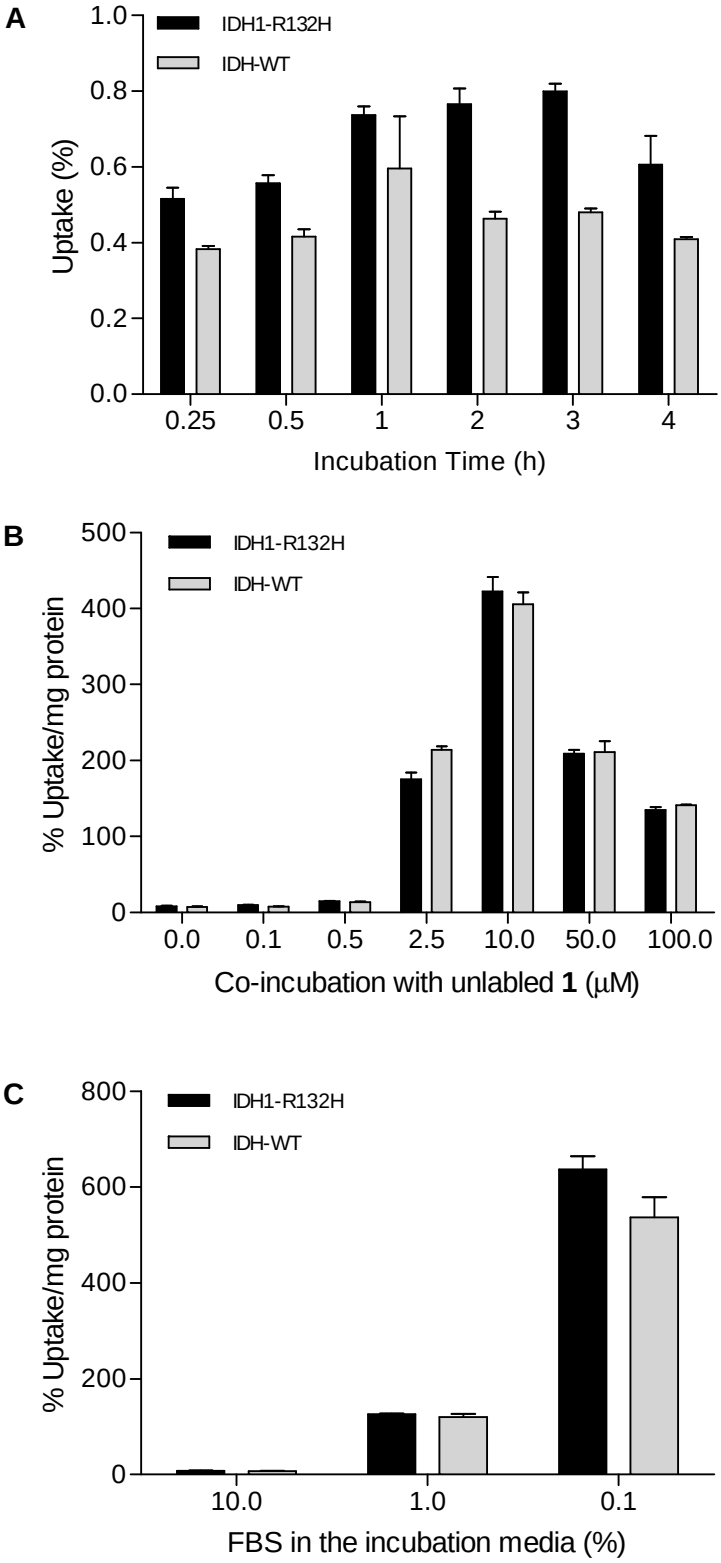
A
IDH1-R132H
IDH-WT
Uptake (%)
1.0
0.8
0.6
0.4
0.2
0.0
0.25
0.5
1
2
3
4
Incubation Time (h)
B
IDH1-R132H
IDH-WT
% Uptake/mg protein
500
400
300
200
100
0
0.0
0.1
0.5
2.5
10.0
50.0
100.0
Co-incubation with unlabled **1** (μM)
C
IDH1-R132H
IDH-WT
% Uptake/mg protein
800
600
400
200
0
10.0
1.0
0.1
FBS in the incubation media (%)

Scheme 1

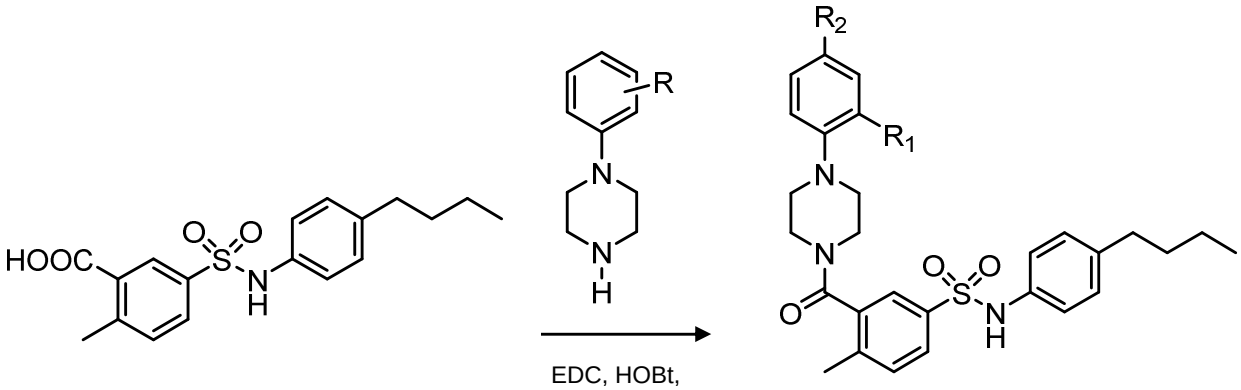

1 R_1 = I, R_2 = H

2 R_1 = H, R_2 = I

4 R_1 = OCH_2CH_2F, R_2 = H

5 R_1 = H, R_2 = OCH_2CH_2F

Scheme 2

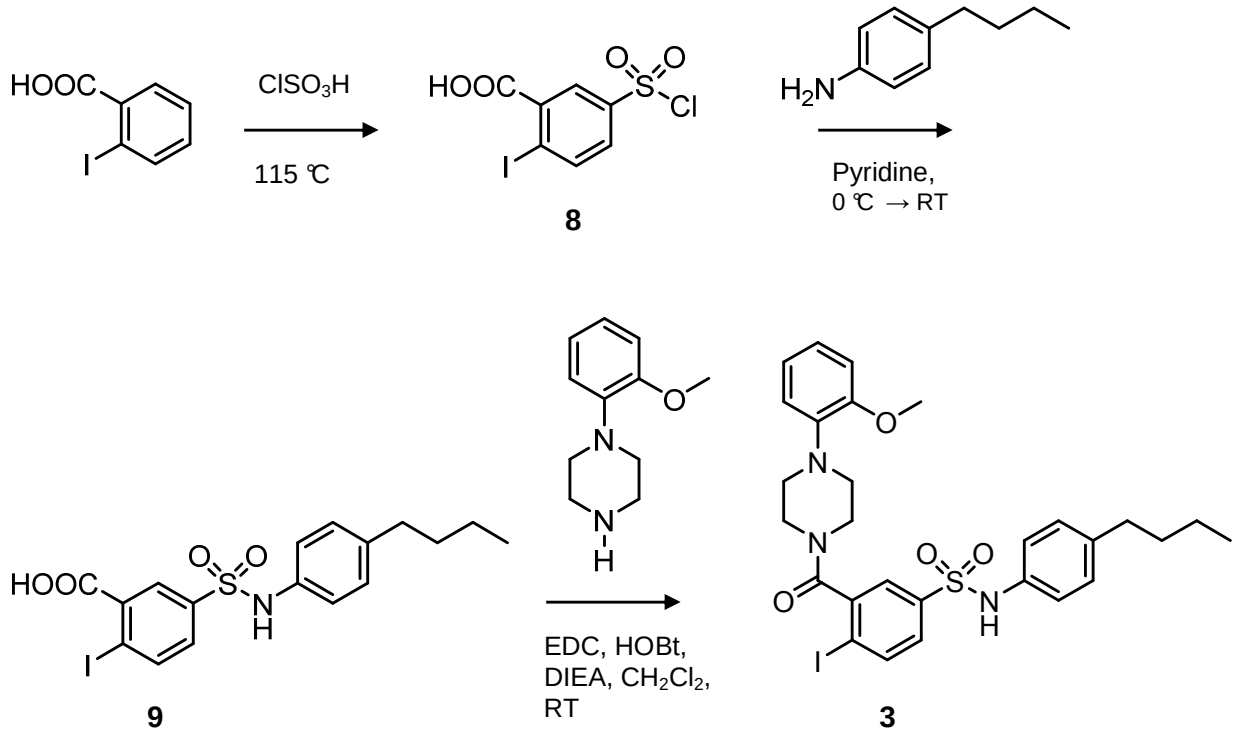
HOOC
I
ClSO3H
115 ℃
HOOC
O
O
S
Cl
I
8
H2N
Pyridine,
0 ℃ → RT
HOOC
O
O
S
N
H
I
9
O
N
N
H
EDC, HOBt,
DIEA, CH2Cl2,
RT
O
N
N
O
O
S
N
H
I
3

Scheme 3

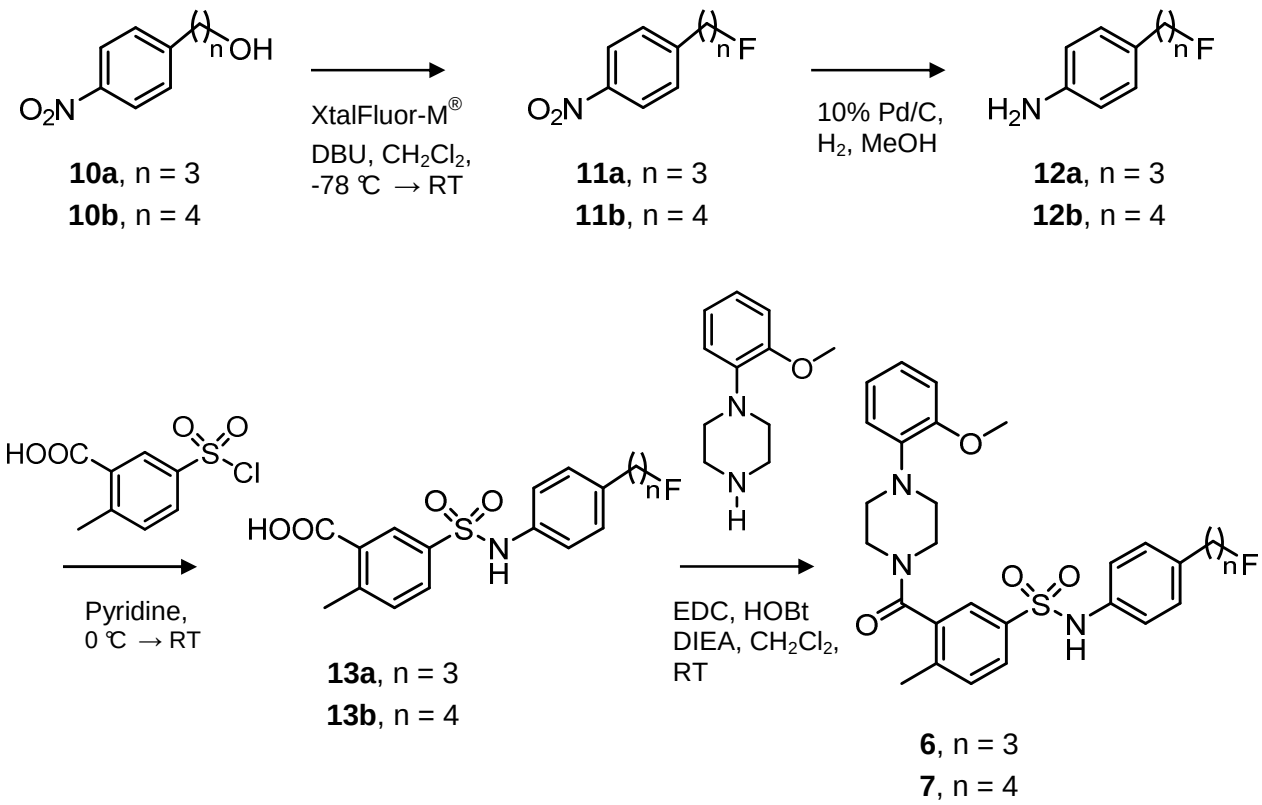

10a, n = 3
10b, n = 4

11a, n = 3
11b, n = 4

12a, n = 3
12b, n = 4

13a, n = 3
13b, n = 4

6, n = 3
7, n = 4

Scheme 4

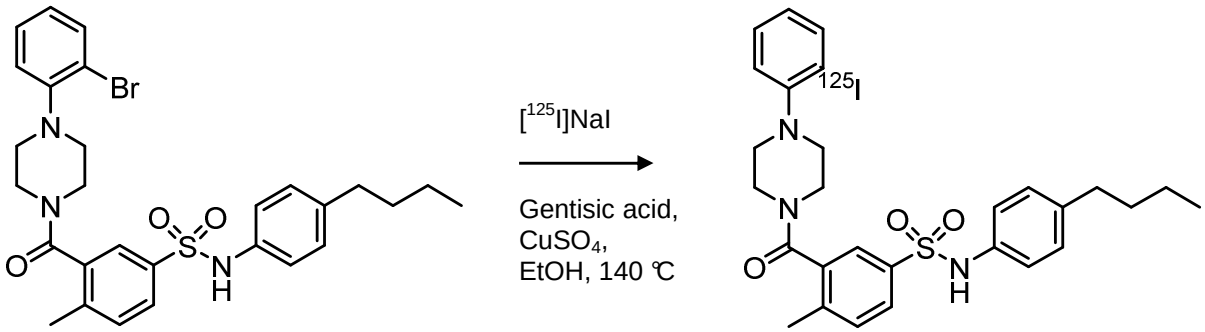

14 **[^{125}I]1**

Scheme 5

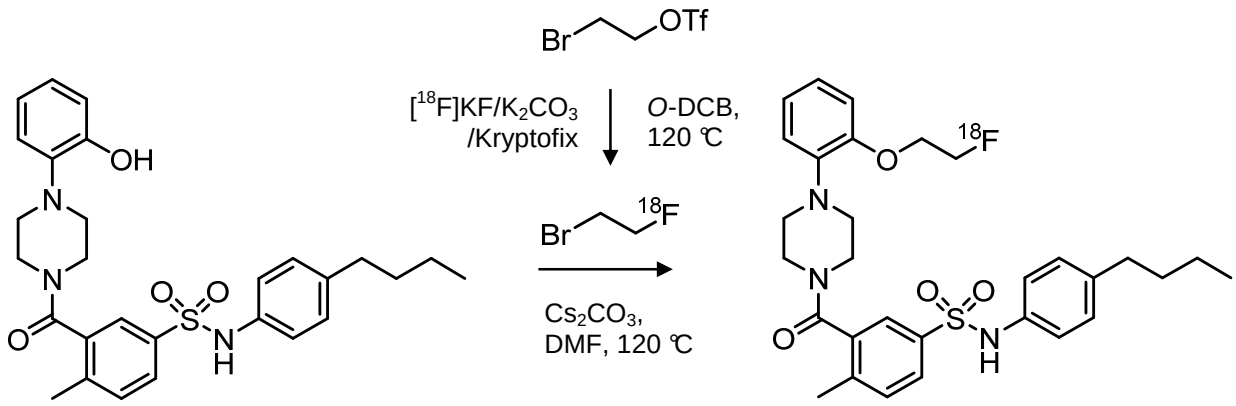

15 **[^{18}F]4**

Table 1. Biodistribution of ^{125}I-labeled **1** in BALB/C mice. Data is presented as percent injected dose (%ID) and as mean ± SD for five animals for each time point.

Organ	5 min	1 h	2 h	4 h
Liver	29.43 ± 5.60	13.30 ± 0.69	6.57 ± 1.77	3.41 ± 0.62
Spleen	0.36 ± 0.12	0.05 ± 0.01	0.03 ± 0.01	0.01 ± 0.01
Lungs	1.69 ± 0.83	0.17 ± 0.02	0.07 ± 0.03	0.03 ± 0.01
Heart	1.11 ± 0.39	0.12 ± 0.02	0.04 ± 0.01	0.01 ± 0.00
Kidneys	3.50 ± 1.08	0.88 ± 0.14	0.43 ± 0.15	0.16 ± 0.03
Bladder	0.03 ± 0.01	0.01 ± 0.01	0.02 ± 0.03	0.01 ± 0.01
Stomach	0.40 ± 0.12	0.65 ± 0.18	0.63 ± 0.82	1.22 ± 2.12
Intestines	6.37 ± 5.80	38.13 ± 1.49	53.24 ± 7.84	41.40 ± 6.02
Thyroid	0.32 ± 0.18	0.04 ± 0.03	0.05 ± 0.05	0.06 ± 0.03
Blood	11.83 ± 1.99	0.71 ± 0.27	0.29 ± 0.09	0.13 ± 0.01
Brain	0.15 ± 0.05	0.03 ± 0.01	0.02 ± 0.01	0.01 ± 0.00
Muscle	13.79 ± 4.85	8.21 ± 0.77	3.91 ± 0.87	1.57 ± 0.34
Bone	3.92 ± 1.45	1.21 ± 0.14	0.60 ± 0.29	0.22 ± 0.14
Skin	3.31 ± 0.74	2.90 ± 1.07	1.25 ± 0.53	0.56 ± 0.09

Research Highlights

- A series of mutant IDH1 enzyme inhibitors were synthesized and evaluated.
- Compounds **1** and **4** exhibited high potency and enzyme inhibition efficiency in vitro.
- **1** and **4** were radiolabeled and evaluated as potential probes for imaging mutant IDH1.
- [^{125}I]**1** displayed favorable tissue distribution characteristics in vivo in normal mice.
- [^{125}I]**1** showed significantly higher uptake in mutant IDH1 tumor cells, and high nonspecific binding was observed at higher concentrations of **1**.